Publ. Astron. Soc. Japan 31, 737-774 (1979)

Global Instability of Polytropic Gaseous Disk Galaxies with Toomre's Density Distribution

Shinko AOKI

Tokyo Astronomical Observatory, University of Tokyo, Mitaka, Tokyo 181

and

Masafumi NOGUCHI and Masanori IYE

Department of Astronomy, Faculty of Science, University of Tokyo, Bunkyo-ku, Tokyo 113

(Received 1979 April 6; revised 1979 June 29)

Abstract

The origin of spiral and/or bar structures of galaxies is studied from a point of view that they are manifestations of gravitationally unstable eigenmodes of galactic disks. Equilibrium models having the surface-density distribution identical to that of Toomre's (1963) first model and with various amount of internal energy due to gaseous pressure of the polytropic exponent $\Gamma=4/3$ are analyzed. By the use of expansion of variables in terms of associated Legendre functions, the problem of small-amplitude oscillations of disk models is reduced to an eigenvalue problem, which is solved numerically.

Main results obtained are summarized as follows: (1) Gaseous pressure generally serves to stabilize the disks. (2) Not only two-armed spiral modes but also one-armed and multi-armed spiral modes as well as ring modes are expected to grow for relatively cool models. (3) The growing spiral patterns are trailing unless the model is extremely cold. (4) There is no tightly wound smooth spiral pattern as far as the most rapidly growing modes are concerned. (5) The amplitude of disturbance undulates significantly along the spiral arms of some modes. (6) The most rapidly growing modes for the first several azimuthal Fourier components have nearly the same pattern speed. The growth time of these modes is comparable with the period of rotation of the system.

Key words: Eigenvalue problem; Global gravitational instability; Polytropic gaseous pressure; Spiral structure; Toomre's disk galaxies.

1. *Introduction*

The origin of spiral and/or bar structures of disk galaxies has long been a riddle for astronomers. In this paper we shall attack this problem from a point of view that they are manifestations of the gravitationally *unstable global* eigenmodes of oscillations of disk galaxies. Before going into detail, we summarize the problem from our point of view.

Since inner parts of disk-shaped galaxies rotate more rapidly than outer parts, it seems that the bar and/or spiral structures of these galaxies will wind up within a few galactic rotations. Morphological properties of these structures, such as the pitch angle of the spiral pattern, the degree of patchiness of arms and so on, are, however, fairly well correlated with some of the global physical quantities of galaxies that cannot vary within a few galactic rotations: for example, the amount of gaseous constituent, the relative extent of the bulge component and the disk component, the total color and so on. Therefore these patterns should be semipersistent even in the presence of differential rotation. This riddle, the so-called winding dilemma, had long been a nuisance for spiral theorists until the well-known density-wave theory was presented by Lin and Shu (1964). By utilizing the WKBJ approximation, they showed that neutral waves of density fluctuation can be persistent in the presence of differential rotation. Though their theory has left a few fundamental problems to be clarified as will be discussed later, it has succeeded in explaining various observational facts (cf. Lin et al. 1969). Furthermore, a concept of galactic shock waves proposed first by Fujimoto (1968) based on the density waves has made an additional advance upon the interpretation of spiral structure. Although there seems to be no direct evidence of the existence of such a density wave and a shock wave, accumulated observational facts as a whole strongly indicate the usefulness of these wave concepts.

Lin–Shu's density wave theory, however, has two basic problems. Firstly, since they utilized the WKBJ approximation, their theory is local and cannot be applied to very long waves strictly. Even if the disk is locally stable, it is not assured that the disk is also stable on the global scale. For self-gravitating systems, the nature of the main force acting in the system, the gravitational force, is essentially of long range. There is no neutralizing effect corresponding to Debye's shield of a plasma composed of charged particles of opposite signs. It is, therefore, essentially necessary to treat the problem of dynamical oscillation of galaxies on the global scale. Secondly, the persistence of neutral spiral waves itself is theoretically questioned from a few different points of view. Toomre (1969) has shown that the waves satisfying Lin–Shu's dispersion relation are inevitably swept away radially with a certain group velocity. Lynden-Bell and Ostriker (1967) have proven the so-called anti-spiral theorem stating that there is no neutral spiral mode unless there exists degeneracy of modes or dissipation mechanism. Lynden-Bell and Kalnajs (1972) have shown that spiral waves transport angular momentum by the gravitational torque and changes the distribution of angular momentum. All these three discussions seriously suspect the existence of purely neutral spiral waves in galaxies. Apart from these discussions, the *neutral* density-wave theory cannot explain convincingly why spiral waves would appear. There are several investigations to obtain unstable spiral modes by the use of a dispersion relation which is obtained by an asymptotic treatment for relatively short waves and is given in the form of a definite integral (cf. Lau et al. 1976). On the other hand, *the global analysis of gravitational instability* is necessary for relatively long-wave modes and might well develop a new insight on the origin of spiral structure, especially of late-type spiral galaxies.

There are two kinds of approach to analyze the global dynamics of galaxies: N-body numerical simulation and linear modal analysis.

Several self-gravitating N-body numerical simulations of the dynamical evolution of stellar disks have been carried out so far (e.g., Miller et al. 1970; Hohl 1971).

These experiments revealed the following general tendency: (1) A self-gravitating stellar disk with a velocity dispersion nearly equal or less than Toomre's (1964) local stability criterion develops a bar-like structure and evolves into a hotter disk. (2) Such a disk sometimes, though not always, develops a temporary spiral structure. However, it does not last more than several periods of rotation. To stabilize these disks, a more massive halo and/or a larger amount of random motions than observed is needed. Although these experiments demonstrate many examples of evolution of stellar disks, they do not yet clarify the basic mechanism of the evolution in detail owing to the complexity of highly non-linear characteristics of the numerical simulations.

Another global approach is the linear modal analysis of disk galaxies. In such a scheme, the pattern speed and the growth rate are uniquely determined for each mode from the eigenvalue of an eigenvalue problem. In comparison with the linear modal analysis of spherical stellar structure, there are a few characteristics peculiar to the problem of disk galaxies. Since the system of a galaxy rotates differentially in general, the main force balancing the gravity is not only the pressure but also the centrifugal force. In such a rotating system, the eigenfrequencies are complex in general even in the case of adiabatic oscillations. The corresponding eigenfunctions possibly involve a complex phase function which may lead to spiral patterns. The configuration of a galaxy is not spherical due to the rotation effect and this fact presents difficulty to solving Poisson's equation exactly.

Hunter (1963) first formulated an approach to this kind of problem intensively. Many subsequent works have been carried out (Hunter 1965; Kalnajs 1972; Bardeen 1975; Iye 1978; Takahara 1978) mainly along his formulation. Erickson (1974) studied the same problem using a different scheme. As for uniformly rotating disks, the problem is rather simple and eigenvalues are obtained analytically in the cases of extremely flattened Maclaurin disks with a particular type of polytropic gaseous pressure. For these models there is no spiral mode and the P_2^2-bar mode remains unstable even if all of the axisymmetric modes are stabilized by the pressure. The results are physically fairly well interpreted. On the other hand, as for differentially rotating disk models, we can derive the following qualitative results common to those modal analyses of several families of disks by Erickson (1974), Bardeen (1975), Iye (1978), and Takahara (1978), although these analyses are carried out entirely numerically under different conditions. There actually exist gravitationally unstable spiral modes unless the disk has a large amount of pressure and/or a massive halo. Spiral modes with a few number of arms grow most rapidly in warm disks, whereas multi-armed modes grow most rapidly in cold disks. The growth time is comparable with the rotation period. The growing modes generally have trailing patterns in the cases of relatively warm disks. Although these results are common to the above-mentioned analyses, we have no proof that they are the universal characteristics. Since it seems very difficult to obtain analytically the global modes of differentially rotating disks, it is desirable to examine the problem for various types of disk models utilizing different approaches and to derive the general characteristics of the problem.

In this paper we study the linear global gravitational stability of the self-gravitating and differentially rotating polytropic gaseous disks of infinite radius. There are a few motives which have led us to examine the stability of infinite disks. Aoki and Iye (1978) have shown that the bi-orthogonalization of surface-

density and potential functions of infinite disks, including non-axisymmetric distributions, results in a compact expression of associated Legendre functions by the use of a special transformation of the coordinates. Expansion of variables in terms of these functions enables us to have a prospective insight into the problem. Furthermore, singular natures of the outer boundary, not removed in the studies by Hunter (1963), Kalnajs (1972), and Iye (1978) for example, are less serious in the case of infinite disks. The infinite disks are more appropriate than finite disks because observed galaxies apparently do not have a sharp outer boundary.

The next section gives the basic equations employed. In section 3, we construct disk models having the surface-density distribution introduced originally by Kuzmin (1956), or that of Toomre's (1963) first model, and having the polytropic pressure distribution. Linearized equations and expansions of variables in terms of associated Legendre functions are given in section 4. As will be discussed in detail in sections 5 and 6, we can reduce the problem to an eigenvalue problem of an infinite matrix. The matrix elements can be obtained, with the use of recurrence formulas given in appendices 1 and 2, very accurately. There is no need to carry out numerical integration. This fact ensures a high numerical accuracy of the present analysis. Section 7 gives the general description of the eigenvalue spectra. The characteristics of several types of modes of interest are given in sections 8 and 9. Discussion and a brief conclusion are given in section 10.

2. *Basic Equations*

The equation of continuity, the equation of motion, and Poisson's equation of gaseous matter confined within a two-dimensional flat space ($z=0$) are written as follows:

$$\frac{\partial \mu}{\partial t}+\boldsymbol{\nabla}\cdot(\mu \boldsymbol{u})=0\ , \tag{2.1}$$

$$\frac{\partial \boldsymbol{u}}{\partial t}+(\boldsymbol{u}\cdot\boldsymbol{\nabla})\boldsymbol{u}+\boldsymbol{\nabla}\phi+\frac{1}{\mu}\boldsymbol{\nabla}P=0\ , \tag{2.2}$$

$$\nabla^2\tilde{\phi}=4\pi G\mu\delta(z)\ , \tag{2.3}$$

where $\boldsymbol{\nabla}$ is the differentiation operator with respect to the two-dimensional space coordinates $\boldsymbol{x}$, $\boldsymbol{u}$ is the velocity at $\boldsymbol{x}$, and μ, ϕ, and P are the surface density, the potential, and the pressure for the two-dimensional space at $\boldsymbol{x}$, respectively, while $\tilde{\phi}$ is the potential in the three-dimensional space, giving ϕ for $z=0$. $\delta(z)$ is Dirac's delta function and G is the gravitational constant. Although P is a tensor in general, we assume here that the pressure P is isotropic within the plane. In particular, assuming that the pressure is barotropic, we can write equation (2.2) as follows:

$$\frac{\partial \boldsymbol{u}}{\partial t}+(\boldsymbol{u}\cdot\boldsymbol{\nabla})\boldsymbol{u}+\boldsymbol{\nabla}\Psi=0\ , \tag{2.2$'$}$$

where Ψ is given by

$$\Psi=\phi+\phi\ , \qquad \phi=\int\frac{dP(\mu)}{\mu}\ , \tag{2.4}$$

ϕ is the apparent potential due to gaseous pressure, and Ψ may be called *effective potential* of our system.

Further, if we assume that the pressure is polytropic,

$$P=K\mu^{\Gamma}\,, \tag{2.5}$$

and we perform the integration in equation (2.4), then we have a power function,

$$\phi=\frac{K\Gamma}{\Gamma-1}\mu^{\Gamma-1}\,. \tag{2.6}$$

Let (r,θ) be the polar coordinates within the (x,y)-plane, then equations (2.1), (2.2′), and (2.3) are rewritten in the Eulerian style as follows:

$$\left.\begin{aligned}
&\frac{\partial\mu}{\partial t}+\frac{1}{r}\frac{\partial(r\mu u)}{\partial r}+\frac{1}{r}\frac{\partial(\mu v)}{\partial\theta}=0\,,\\
&\frac{\partial u}{\partial t}+u\frac{\partial u}{\partial r}+\frac{v}{r}\frac{\partial u}{\partial\theta}-\frac{v^2}{r}+\frac{\partial\Psi}{\partial r}=0\,,\\
&\frac{\partial v}{\partial t}+u\frac{\partial v}{\partial r}+\frac{v}{r}\frac{\partial v}{\partial\theta}+\frac{uv}{r}+\frac{1}{r}\frac{\partial\Psi}{\partial\theta}=0\,,\\
&\frac{1}{r}\frac{\partial}{\partial r}\left(r\frac{\partial\tilde{\phi}}{\partial r}\right)+\frac{1}{r^2}\frac{\partial^2\tilde{\phi}}{\partial\theta^2}+\frac{\partial^2\tilde{\phi}}{\partial z^2}=4\pi G\mu\delta(z)\,,
\end{aligned}\right\} \tag{2.7}$$

where u and v are the radial and tangential (perpendicular to the radius vector) velocity components at the point (r,θ), respectively.

3. *An Equilibrium Solution*

We adopt Toomre's (1963) first model, as an equilibrium solution for computational simplicity, given by

$$\phi_0=-\frac{GM}{a}\left(\frac{1-\xi}{2}\right)^{1/2}\,,\qquad \mu_0=\frac{M}{2\pi a^2}\left(\frac{1-\xi}{2}\right)^{3/2}\,, \tag{3.1}$$

where

$$\xi=(r^2-a^2)/(r^2+a^2)\,. \tag{3.1′}$$

The subscript zero stands for the equilibrium solution. The expression of $\Psi_0=\phi_0+\phi_0$ corresponding to the surface density μ_0 is deduced from equations (2.4), (2.6), and (3.1), and is given explicitly by

$$\Psi_0=-\frac{GM}{a}\left(\frac{1-\xi}{2}\right)^{1/2}+\frac{K\Gamma}{\Gamma-1}\left(\frac{M}{2\pi a^2}\right)^{\Gamma-1}\left(\frac{1-\xi}{2}\right)^{3(\Gamma-1)/2}\,. \tag{3.2}$$

Assuming that $(\partial/\partial t)=(\partial/\partial\theta)=0$ for the equilibrium solution, we obtain, from equations (2.7),

$$\left.\begin{aligned}
&u_0=0\,,\\
&v_0^2=V^2\equiv r\frac{d\Psi_0}{dr}\,,
\end{aligned}\right\} \tag{3.3}$$

where V is the rotation velocity. Or explicitly, we have

$$V^2=\frac{GM}{a}\left(\frac{1-\xi}{2}\right)^{1/2}\left(\frac{1+\xi}{2}\right)\left[1-\varepsilon_\Gamma\left(\frac{1-\xi}{2}\right)^{3\Gamma/2-2}\right], \tag{3.4}$$

where

$$\varepsilon_\Gamma=(3aK\Gamma/GM)(M/2\pi a^2)^{\Gamma-1}. \tag{3.5}$$

Therefore, for $\Gamma<4/3$, the value of the right-hand side of equation (3.4) is negative for ξ in a domain given by

$$\xi_{\rm crit}<\xi\leqq 1, \tag{3.6}$$

where

$$\xi_{\rm crit}=\max\{-1, 1-2(\varepsilon_\Gamma)^{1/(2-3\Gamma/2)}\}, \tag{3.7}$$

and then V cannot be defined to be a real quantity. Physically speaking, this situation corresponds to the fact that the pressure term prevails over the gravitational force in the outer part of the disk given by expression (3.6), so that we cannot obtain a real global equilibrium solution for $0\leqq r<\infty$ in the case of Toomre's (1963) first model. This fact is already pointed out by Aoki (1965). On the contrary, for $\Gamma\geqq 4/3$, we do not have such a restriction provided

$$\varepsilon_\Gamma\leqq 1. \tag{3.8}$$

In this connection, we confine ourselves for simplicity to consider only the case of

$$\Gamma=4/3, \tag{3.9}$$

as a limiting case physically permitted from the above restriction. Denoting ε for $\varepsilon_{4/3}$, namely,

$$\varepsilon=(4Ka/GM)(M/2\pi a^2)^{1/3}, \tag{3.10}$$

we have the effective potential of the present model, Ψ_0, and the equilibrium angular rotation velocity, Ω, given by

$$\Psi_0=-(1-\varepsilon)(GM/a)[(1-\xi)/2]^{1/2}, \tag{3.11}$$

$$\Omega\equiv V/r=(1-\varepsilon)^{1/2}(GM/a^3)^{1/2}[(1-\xi)/2]^{3/4}. \tag{3.12}$$

μ_0 and v_0 are indicated in figures 1a and 1b, respectively.

In order to clarify the physical meaning of ε, we calculate the following integrated quantities: The total kinetic energy T_0 due to rotation (or organized motion) is given by

$$T_0=\int_0^{2\pi}\int_0^{\infty}\frac{1}{2}V^2\mu_0 r dr d\theta=\frac{(1-\varepsilon)GM^2}{8a}. \tag{3.13}$$

The total potential energy is

$$W_0=\frac{1}{2}\int_0^{2\pi}\int_0^{\infty}\phi_0\mu_0 r dr d\theta=-\frac{GM^2}{4a}. \tag{3.14}$$

Since the degree of freedom is 2, the total internal energy (or the total kinetic energy due to random motion) is

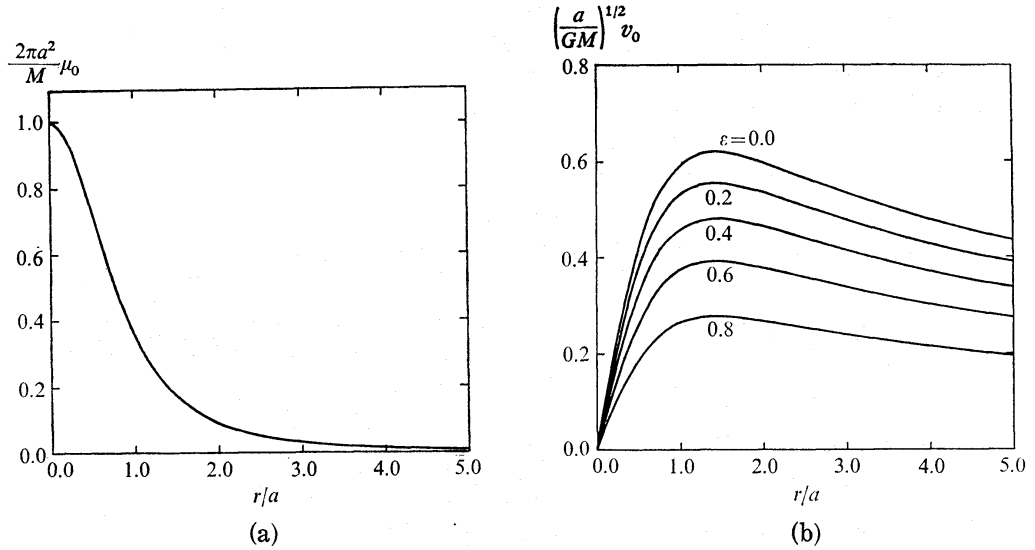

Fig. 1. (a) Surface-density distribution of the equilibrium disk models defined by equation (3.1).

(b) Rotation velocity of the equilibrium disk models. These curves have the same functional form but the different numerical factors, and attain their maximum at $r=2^{1/2}a$. The curve for the model with $\varepsilon=1.0$ coincides with the r/a-axis.

$$U_0=\int_0^{2\pi}\int_0^{\infty}P_0 r dr d\theta=\frac{\varepsilon GM^2}{8a}\,. \tag{3.15}$$

Therefore, since the total energy E_0 is given by

$$E_0=T_0+U_0+W_0=-\frac{GM^2}{8a}\,, \tag{3.16}$$

ε is given by

$$\varepsilon=(\text{internal energy})/|(\text{total energy})|\,, \tag{3.17}$$

and the virial theorem is satisfied in the form,

$$2(T_0+U_0)+W_0=0\,. \tag{3.18}$$

On the other hand, Ostriker and Peebles (1973) introduced a quantity t,

$$t=(\text{organized kinetic energy})/|(\text{potential energy})|\,, \tag{3.19}$$

in order to obtain a stability criterion, and also Bardeen (1975) examined the stability using this quantity. The relation between our ε and t is given by the equation,

$$t=(1-\varepsilon)/2\,, \tag{3.20}$$

and β introduced by Iye (1978) is the same as ε introduced here. Note that we can choose a self-consistent model with any value of ε satisfying $0\leqq\varepsilon\leqq1$, while polytropic models with a finite radius investigated by Iye (1978) and by Takahara (1978) are restricted to a narrow range of ε.

4. *Linear Self-Gravitating Disturbances*

In order to obtain possible global patterns of the spiral structure of galaxies, we study the stability or the instability of the equilibrium disks against infinitesimal deviations. For this purpose it is convenient to use the bi-orthogonal relation between the surface-density and the potential functions derived by Aoki and Iye (1978). They have shown that, if μ is expansible in the form

$$\mu=\frac{M}{2\pi a^2}\left(\frac{1-\xi}{2}\right)^{3/2}\sum_{m=-\infty}^{\infty}\sum_{n=|m|}^{\infty}a_n{}^m\hat{P}_n{}^{|m|}(\xi)\exp(im\theta)\,, \tag{4.1}$$

then the corresponding potential required by Poisson's equation (2.3) is given by

$$\phi=-\frac{GM}{a}\left(\frac{1-\xi}{2}\right)^{1/2}\sum_{m=-\infty}^{\infty}\sum_{n=|m|}^{\infty}\frac{a_n{}^m}{2n+1}\hat{P}_n{}^{|m|}(\xi)\exp(im\theta)\,, \tag{4.2}$$

where $\hat{P}_n{}^{|m|}(\xi)$ is the orthonormal associated Legendre function given by

$$\hat{P}_n{}^{|m|}(\xi)=\left[\frac{(n-|m|)!}{(n+|m|)!}\frac{(2n+1)}{2}\right]^{1/2}P_n{}^{|m|}(\xi)\,. \tag{4.3}$$

They have further suggested the following:

PROPOSITION. *Let S be a self-adjoint operator to yield the potential ϕ by applying it to the surface density μ*

$$\phi=S\mu\,, \tag{4.4}$$

or explicitly

$$\phi(r,\theta)=-\int_0^{2\pi}\int_0^{\infty}[r^2+(r')^2-2rr'\cos(\theta-\theta')]^{-1/2}\mu(r',\theta')r'dr'd\theta'\,. \tag{4.4'}$$

If and only if μ satisfies the condition,

$$-\int_0^{2\pi}\int_0^{\infty}\mu^*S\mu r dr d\theta<\infty\,, \tag{4.5}$$

where the asterisk stands for the complex conjugate, μ is expansible in the form (4.1) and the corresponding potential is given by equation (4.2). Further the left-hand side of inequality (4.5) is written in terms of Fourier coefficients $a_n{}^m$'s in the form,

$$-\int_0^{2\pi}\int_0^{\infty}\mu^*\phi r dr d\theta=+\frac{GM^2}{4a}\sum_{m=-\infty}^{\infty}\sum_{n=|m|}^{\infty}\frac{|a_n{}^m|^2}{2n+1}\,. \tag{4.6}$$

The meaning of the convergence in equations (4.1) and (4.2) is given by equation (4.20) of Aoki and Iye (1978).

The above proposition is not yet mathematically proven. On the other hand, we may say that condition (4.5) is less restrictive enough for physical applications. In this respect, it is interesting that *any* kind of distribution μ expressing the physical surface-density distribution of disk galaxies would be expansible if the proposition is true; in other words, though bi-orthogonalized Toomre's surface-density functions have a particular common factor

$$\left(\frac{1-\xi}{2}\right)^{3/2}=\left(\frac{a^2}{r^2+a^2}\right)^{3/2}, \tag{4.7}$$

yet they would constitute a representative system of the bases for the functional space of μ under condition (4.5).

Since the relation between the potential and the surface density is linear, we can solve *linearized* Poisson's equation exactly, i.e., we may interpret that equations (4.1) and (4.2) give the expressions for disturbances, the deviations from the equilibrium solution given by equation (3.1). In the linearized equations, we may take up the disturbances of different m's separately. Similarly, the time dependency may be expressed by the factor $\exp(-i\omega t)$. Thus we use the expressions,

$$\left.\begin{aligned}
\mu&=\mu_0+\mu'\exp(im\theta-i\omega t)\,,\\
\phi&=\phi_0+\phi'\exp(im\theta-i\omega t)\,,\\
u&=\quad u'\exp(im\theta-i\omega t)\,,\\
v&=v_0+v'\exp(im\theta-i\omega t)\,,\\
\phi&=\phi_0+\phi'\exp(im\theta-i\omega t)\,.
\end{aligned}\right\} \tag{4.8}$$

Now, since we obtain

$$\begin{aligned}
\phi&=\frac{\varepsilon GM}{a}\left(\frac{M}{2\pi a^2}\right)^{-1/3}\mu^{1/3}\\
&=\frac{\varepsilon GM}{a}\left(\frac{1-\xi}{2}\right)^{1/2}\left[1+\frac{\mu'\exp(im\theta-i\omega t)}{3\mu_0}\right],
\end{aligned} \tag{4.9}$$

from equations (2.6), (3.9), (3.10), and the first of equations (4.8), we obtain the expression,

$$\phi'=\frac{\varepsilon}{3}\left(\frac{GM}{a}\right)\left(\frac{1-\xi}{2}\right)^{1/2}\frac{\mu'}{\mu_0}\,. \tag{4.10}$$

Thus inserting equations (4.8) into equations (2.7) except for Poisson's equation already solved, we obtain the linearized equations:

$$\left.\begin{aligned}
&i(-\omega+m\Omega)\mu'+\frac{1}{r}\frac{d}{dr}(r\mu_0u')+\frac{im\mu_0v'}{r}=0\,,\\
&\frac{d\Psi'}{dr}+i(-\omega+m\Omega)u'-2\Omega v'=0\,,\\
&im\frac{\Psi'}{r}+\frac{\kappa^2}{2\Omega}u'+i(-\omega+m\Omega)v'=0\,,
\end{aligned}\right\} \tag{4.11}$$

where Ψ' is the disturbance of Ψ:

$$\Psi=\Psi_0+\Psi'\,,\qquad \Psi'=\phi'+\phi'\,, \tag{4.12}$$

and κ is the so-called epicyclic frequency defined by

$$\kappa^2=4\Omega^2[1+(1/2)(r/\Omega)d\Omega/dr]\,. \tag{4.13}$$

For Ω given by equation (3.12), we obtain

$$\frac{\kappa^2}{2\Omega}=(1-\varepsilon)^{1/2}\left(\frac{GM}{a^3}\right)^{1/2}\left(\frac{1-\xi}{2}\right)^{3/4}\left[\frac{1}{2}+\frac{3}{2}\left(\frac{1-\xi}{2}\right)\right]. \tag{4.14}$$

Now, we adopt the following expansions:

$$\left.\begin{aligned}
\mu' &= \frac{M}{2\pi a^2}\left(\frac{1-\xi}{2}\right)^{3/2}\sum_{n=|m|}^{\infty} a_n{}^m \hat{P}_n{}^{|m|}(\xi)\,,\\
\phi' &= -\frac{GM}{a}\left(\frac{1-\xi}{2}\right)^{1/2}\sum_{n=|m|}^{\infty}\frac{a_n{}^m}{2n+1}\hat{P}_n{}^{|m|}(\xi)\,,\\
\Psi' &= \phi'+\phi'\\
&= -\frac{GM}{a}\left(\frac{1-\xi}{2}\right)^{1/2}\sum_{n=|m|}^{\infty}\left(\frac{1}{2n+1}-\frac{\varepsilon}{3}\right)a_n{}^m\hat{P}_n{}^{|m|}(\xi)\,.
\end{aligned}\right\} \tag{4.15}$$

We introduce further the dimensionless quantities,

$$\hat{\omega}=\left(\frac{GM}{a^3}\right)^{-1/2}\omega\,,\qquad \hat{\Omega}=\left(\frac{GM}{a^3}\right)^{-1/2}\Omega\,,\qquad \hat{\kappa}=\left(\frac{GM}{a^3}\right)^{-1/2}\kappa\,, \tag{4.16}$$

in order to obtain the dimensionless equations in the following.

5. *Eigenequation and Its Matrix Elements for Non-axisymmetric Cases* ($m\neq 0$)

First we take up the case of $m\neq 0$, and introduce tentatively the expansion schemes of u' and v',

$$\left.\begin{aligned}
u' &= i\,\mathrm{sign}\,(m)\left(\frac{GM}{a}\right)^{1/2}\left(\frac{1-\xi}{2}\right)^{1/4}\left(\frac{1+\xi}{2}\right)^{-1/2}\sum_{n=|m|}^{\infty} b_n{}^m\hat{P}_n{}^{|m|}(\xi)\,,\\
v' &= \left(\frac{GM}{a}\right)^{1/2}\left(\frac{1-\xi}{2}\right)^{1/4}\left(\frac{1+\xi}{2}\right)^{-1/2}\sum_{n=|m|}^{\infty} c_n{}^m\hat{P}_n{}^{|m|}(\xi)\,,
\end{aligned}\right\} \tag{5.1}$$

where

$$\mathrm{sign}\,(m)=m/|m|\,. \tag{5.2}$$

Inserting equations (4.15) and (5.1) into equations (4.11), and using the orthogonality relations among the associated Legendre functions, we obtain a system of linear equations for $a_n{}^m$, $b_n{}^m$, and $c_n{}^m$ with eigenvalue $\mathrm{sign}\,(m)\,\hat{\omega}$. Expressing it in a matrix form, we have

$$\begin{pmatrix} A & B & C\\ D & A & F\\ G & H & A\end{pmatrix}\begin{pmatrix}\boldsymbol{a}\\ \boldsymbol{b}\\ \boldsymbol{c}\end{pmatrix}=\lambda\begin{pmatrix}\boldsymbol{a}\\ \boldsymbol{b}\\ \boldsymbol{c}\end{pmatrix},\qquad \lambda=\mathrm{sign}\,(m)\,\hat{\omega}\,, \tag{5.3}$$

where $\boldsymbol{a}$, $\boldsymbol{b}$, and $\boldsymbol{c}$ are themselves vectors defined by

$$\boldsymbol{a}=\begin{pmatrix} a^m_{|m|}\\ a^m_{|m|+1}\\ a^m_{|m|+2}\\ \vdots\end{pmatrix},\qquad \boldsymbol{b}=\begin{pmatrix} b^m_{|m|}\\ b^m_{|m|+1}\\ b^m_{|m|+2}\\ \vdots\end{pmatrix},\qquad \boldsymbol{c}=\begin{pmatrix} c^m_{|m|}\\ c^m_{|m|+1}\\ c^m_{|m|+2}\\ \vdots\end{pmatrix}. \tag{5.4}$$

A, B, C, D, F, G, and H are matrices and their (l, n)-elements are expressed by the following formulas:

$$A_{ln}=|m|\int_{-1}^{1}\hat{P}_l^{|m|}\hat{\Omega}(\xi)\hat{P}_n^{|m|}d\xi\,, \tag{5.5}$$

$$B_{ln}=4\int_{-1}^{1}\hat{P}_l^{|m|}\left(\frac{1-\xi}{2}\right)^{1/2}\frac{d}{d\xi}\left[\left(\frac{1-\xi}{2}\right)^{5/4}\hat{P}_n^{|m|}\right]d\xi\,, \tag{5.6}$$

$$C_{ln}=|m|\int_{-1}^{1}\hat{P}_l^{|m|}\left(\frac{1-\xi}{2}\right)^{3/4}\left(\frac{1+\xi}{2}\right)^{-1}\hat{P}_n^{|m|}d\xi\,, \tag{5.7}$$

$$D_{ln}=4\left(\frac{1}{2n+1}-\frac{\varepsilon}{3}\right)\int_{-1}^{1}\hat{P}_l^{|m|}\left(\frac{1-\xi}{2}\right)^{5/4}\left(\frac{1+\xi}{2}\right)\frac{d}{d\xi}\left[\left(\frac{1-\xi}{2}\right)^{1/2}\hat{P}_n^{|m|}\right]d\xi\,, \tag{5.8}$$

$$F_{ln}=2\int_{-1}^{1}\hat{P}_l^{|m|}\hat{\Omega}\hat{P}_n^{|m|}d\xi\,, \tag{5.9}$$

$$G_{ln}=-|m|\left(\frac{1}{2n+1}-\frac{\varepsilon}{3}\right)\int_{-1}^{1}\hat{P}_l^{|m|}\left(\frac{1-\xi}{2}\right)^{3/4}\hat{P}_n^{|m|}d\xi\,, \tag{5.10}$$

$$H_{ln}=\int_{-1}^{1}\hat{P}_l^{|m|}(\hat{\kappa}^2/2\hat{\Omega})\hat{P}_n^{|m|}d\xi\,, \tag{5.11}$$

where $\hat{P}_n^{|m|}$ stands for $\hat{P}_n^{|m|}(\xi)$.

Since the values of coefficients A, B, $\cdots$, H are invariant under the transformation $m\to -m$, $\boldsymbol{a}$, $\boldsymbol{b}$, and $\boldsymbol{c}$ remain unaltered, namely

$$a_n{}^{-m}=a_n{}^{m}\,, \tag{5.12}$$

and so on, provided that $\hat{\omega}$ changes sign: $\hat{\omega}\to-\hat{\omega}$. As seen from equations (4.8), m and ω appear always in a combined form $\exp(im\theta-i\omega t)$. Besides, since the matrix elements in the left-hand side of equation (5.3) are all real, we obtain solutions for ω in a conjugate pair:

$$\omega=\omega_{\mathrm{R}}\pm i|\omega_{\mathrm{I}}| \qquad \text{for} \qquad |\omega_{\mathrm{I}}|\neq 0\,, \tag{5.13}$$

where ω_{R} and ω_{I} are the real and imaginary parts of ω, respectively. Therefore, for a fixed $|m|\neq 0$, we have a quartet of solutions:

$$\left.\begin{aligned}
&a_n{}^{|m|}\exp(|\omega_{\mathrm{I}}|t)\exp[i(|m|\theta-\omega_{\mathrm{R}}t)]\,,\\
&a_n{}^{|m|}\exp(-|\omega_{\mathrm{I}}|t)\exp[-i(|m|\theta-\omega_{\mathrm{R}}t)]\,,\\
&(a_n{}^{|m|})^*\exp(|\omega_{\mathrm{I}}|t)\exp[-i(|m|\theta-\omega_{\mathrm{R}}t)]\,,\\
&(a_n{}^{|m|})^*\exp(-|\omega_{\mathrm{I}}|t)\exp[i(|m|\theta-\omega_{\mathrm{R}}t)]\,,
\end{aligned}\right\} \tag{5.14}$$

and so on for $\boldsymbol{b}$ and $\boldsymbol{c}$, where the asterisk stands for the complex conjugate. Keeping in mind this fact, we may calculate only for $m>0$, because we can derive the other solutions easily whenever they are needed. Therefore, we restrict ourselves in this section to the case where

$$m>0\,, \tag{5.15}$$

and omit the absolute sign in associated Legendre functions. It is also noted

that, if the growing solutions given by the first and third of expressions (5.14) represent a trailing spiral pattern for example, then the decaying solutions by the second and fourth expressions represent a leading pattern.

We introduce here the following expressions:

$$\hat{I}(\alpha, m; l, n) = \int_{-1}^{1} \left(\frac{1-\xi}{2}\right)^{\alpha} \hat{P}_l^m \hat{P}_n^m d\xi , \tag{5.16}$$

$$\hat{J}(\alpha, m; l, n) = \int_{-1}^{1} \left(\frac{1-\xi}{2}\right)^{\alpha} \left(\frac{1+\xi}{2}\right)^{-1} \hat{P}_l^m \hat{P}_n^m d\xi . \tag{5.17}$$

The matrix elements given by equations (5.5)-(5.11) are expressed by these expressions $\hat{I}$ and $\hat{J}$ only for $\alpha=3/4$ and 7/4. Moreover, $\hat{I}$'s are calculated by successive applications of recurrence formulas starting from $l=n=m$. As for $\hat{J}$'s the starting expressions are for $n=m$, $l=m$ and for $n=m$, $l=m+1$. They are all calculated with the aid of Beta functions analytically. The derivations of the recurrence formulas are given in appendix 1, and the final forms are given by equations (A.18)-(A.21) for $\hat{I}$, and by equations (A.24)-(A.28) for $\hat{J}$.

The explicit formulas of the matrix elements (5.5)-(5.11) in terms of $\hat{I}$ and $\hat{J}$ are, for $m>0$,

$$A_{ln} = m(1-\varepsilon)^{1/2} \hat{I}\left(\frac{3}{4}, m; l, n\right), \tag{5.18}$$

$$B_{ln} = \frac{1}{2}\left\{\left[\frac{(2l+1)(l+m+1)(l-m+1)}{2l+3}\right]^{1/2} \hat{J}\left(\frac{3}{4}, m; l+1, n\right) + \hat{J}\left(\frac{3}{4}, m; l, n\right) - \left[\frac{(2l+1)(l+m)(l-m)}{2l-1}\right]^{1/2} \hat{J}\left(\frac{3}{4}, m; l-1, n\right)\right\}, \tag{5.19}$$

$$C_{ln} = m\hat{J}\left(\frac{3}{4}, m; l, n\right), \tag{5.20}$$

$$D_{ln} = \frac{1}{2}\left(\frac{1}{2n+1} - \frac{\varepsilon}{3}\right)\left\{-\left[\frac{(2n+1)(n+m+1)(n-m+1)}{2n+3}\right]^{1/2} \hat{I}\left(\frac{3}{4}, m; l, n+1\right) - \hat{I}\left(\frac{3}{4}, m; l, n\right) + \left[\frac{(2n+1)(n+m)(n-m)}{2n-1}\right]^{1/2} \hat{I}\left(\frac{3}{4}, m; l, n-1\right)\right\}, \tag{5.21}$$

$$F_{ln} = 2(1-\varepsilon)^{1/2} \hat{I}\left(\frac{3}{4}, m; l, n\right), \tag{5.22}$$

$$G_{ln} = -m\left(\frac{1}{2n+1} - \frac{\varepsilon}{3}\right) \hat{I}\left(\frac{3}{4}, m; l, n\right), \tag{5.23}$$

$$H_{ln} = \frac{1}{2}(1-\varepsilon)^{1/2}\left[\hat{I}\left(\frac{3}{4}, m; l, n\right) + 3\hat{I}\left(\frac{7}{4}, m; l, n\right)\right]. \tag{5.24}$$

6. *Axisymmetric Case* ($m=0$)

The expansions for u' and v' given in equations (5.1) have some difficulty

for $m=0$ at $r=0$ (or $\xi=-1$), since they have singularities there unless

$$\left.\begin{aligned}\sum_{n=0}^{\infty} b_n\hat{P}_n(\xi) &\to \left(\frac{1+\xi}{2}\right)^{1/2}\times\text{constant}\,,\\ \sum_{n=0}^{\infty} c_n\hat{P}_n(\xi) &\to \left(\frac{1+\xi}{2}\right)^{1/2}\times\text{constant}\,,\end{aligned}\right\} \tag{6.1}$$

as

$$\xi\to -1\,.$$

Therefore, we have altered the expansion series in order to avoid these singularities as follows:

$$\left.\begin{aligned}u' &= i\left(\frac{GM}{a}\right)^{1/2}\left(\frac{1-\xi}{2}\right)^{-1/2}\left(\frac{1+\xi}{2}\right)^{1/2}\sum_{n=0}^{\infty} b_n\hat{P}_n(\xi)\,,\\ v' &= \left(\frac{GM}{a}\right)^{1/2}\left(\frac{\hat{\kappa}^2}{2\hat{\Omega}}\right)\left(\frac{1-\xi}{2}\right)^{-1/2}\left(\frac{1+\xi}{2}\right)^{1/2}\sum_{n=0}^{\infty} c_n\hat{P}_n(\xi)\,.\end{aligned}\right\} \tag{6.2}$$

The other expansions given by equations (4.15) are unaltered, except for the omission of the unnecessary superscripts m or $|m|$. It is noted that

$$A=C=G=O\,, \tag{6.3}$$

owing to the factor m. Thus we obtain instead of equation (5.3) a matrix equation with eigenvalue $\hat{\omega}$,

$$\begin{pmatrix} O & B & O\\ D & O & F\\ O & H & O\end{pmatrix}\begin{pmatrix}\boldsymbol{a}\\ \boldsymbol{b}\\ \boldsymbol{c}\end{pmatrix}=\hat{\omega}\begin{pmatrix}\boldsymbol{a}\\ \boldsymbol{b}\\ \boldsymbol{c}\end{pmatrix}, \tag{6.4}$$

where the matrix elements are given by

$$\left.\begin{aligned}B_{ln} &= 4\int_{-1}^{1}\hat{P}_l\left(\frac{1-\xi}{2}\right)^{1/2}\frac{d}{d\xi}\left[\left(\frac{1-\xi}{2}\right)^{1/2}\left(\frac{1+\xi}{2}\right)\hat{P}_n\right]d\xi\,,\\ D_{ln} &= 4\left(\frac{1}{2n+1}-\frac{\varepsilon}{3}\right)\int_{-1}^{1}\hat{P}_l\left(\frac{1-\xi}{2}\right)^{2}\frac{d}{d\xi}\left[\left(\frac{1-\xi}{2}\right)^{1/2}\hat{P}_n\right]d\xi\,,\\ F_{ln} &= (1-\varepsilon)\int_{-1}^{1}\hat{P}_l\left(\frac{1-\xi}{2}\right)^{3/2}\left[1+3\left(\frac{1-\xi}{2}\right)\right]\hat{P}_n d\xi\,,\\ H_{ln} &= \delta_{ln}\,,\end{aligned}\right\} \tag{6.5}$$

where δ_{ln} is Kronecker's delta.

The series expansions given by equations (6.2) can also be justified, since they satisfy automatically the mass-conservation requirement in the sense that there is neither source nor sink at $r=0$ and $r=\infty$; in fact we have

$$\left.\begin{aligned}\frac{d}{dt}\int_0^{\infty}\mu' r dr &= -\int_0^{\infty}\frac{1}{r}\frac{d}{dr}(r\mu_0 u')r dr = -[r\mu_0 u']_0^{\infty}\\ &= \frac{iM}{2\pi a}\left(\frac{GM}{a}\right)^{1/2}\left[-\left(\frac{1-\xi}{2}\right)^{1/2}\left(\frac{1+\xi}{2}\right)\sum_{n=0}^{\infty} b_n\hat{P}_n(\xi)\right]_{-1}^{1}\\ &= 0\,,\end{aligned}\right\} \tag{6.6}$$

provided that

$$|\sum b_n \hat{P}_n(\xi)| < \infty \,, \qquad \text{for} \quad \xi = \pm 1 \,. \tag{6.7}$$

The matrix elements for equation (6.4) can be calculated by using the quantities given in appendix 1. We can, however, have a more compact form for the equation to be solved, owing to the peculiar form of equation (6.4), given by

$$(BD + BFB^{-1})\boldsymbol{a} = (\hat{\omega})^2 \boldsymbol{a} \,, \tag{6.8}$$

provided that

$$\hat{\omega} \neq 0 \,. \tag{6.9}$$

Matrix elements for B^{-1}, BD, and BF are given in appendix 2, explicitly by equations (A.42), (A.46), and (A.48), respectively.

As for $\hat{\omega}=0$, we obtain the reduced forms,

$$\left.\begin{aligned} B\boldsymbol{b} &= 0 \,, \\ D\boldsymbol{a} + F\boldsymbol{c} &= 0 \,, \\ \boldsymbol{b} &= 0 \,. \end{aligned}\right\} \tag{6.10}$$

The first and the third equations give

$$u' = 0 \,, \tag{6.10'}$$

and the second equation shows that a different equilibrium solution from the one given by equations (3.1) also exists provided that the rotation velocity is properly chosen for any given potential according to the corresponding surface-density function. This is physically evident. Comparing the form of equation (6.8) where $\hat{\omega}$ enters in the form $(\hat{\omega})^2$ and the form of equation (6.4), we may state that one-third of the total eigenvalues belong to the self-evident equilibrium solutions given by equations (6.10), while the other two-thirds should satisfy equation (6.8). Note that even within the two-thirds there may exist an equilibrium solution where $\hat{\omega}=0$; this is a case of fortuitous degeneracy.

The superiority of the form (6.8) to the form (6.4) comes from the following reasons:

(1) the self-evident equilibrium cases given by equations (6.10) are excluded;

(2) the eigenvalues are given in pairs,

$$\hat{\omega} \text{ and } -\hat{\omega} \,;$$

(3) we may extend the number of terms in the expansion by three times, using the same size of memory of computer in solving the eigenvalue problem numerically; and

(4) moreover, the necessary matrix elements are explicitly given as in appendix 2, although they have apparently complicated forms at a first glance.

7. *Eigenvalue Spectra*

Eigenequation (5.3) for $m=1, 2, 3$, and 4, and eigenequation (6.8) for $m=0$ are solved numerically for several values of ε. We expand μ', ϕ', Ψ', u', and v' in terms of 25 terms (up to $n=m+24$), respectively, in the non-axisymmetric case and calculate 75 eigenvalues and 75 eigenvectors for each m and for each ε. In addition, a calculation using 20-term expansion is performed in order to see

the numerical accuracy of obtained results. Since equation (6.8) allows three times the number of terms in the expansion [see statement (3) in section 6], we examine expansions by 50 and 75 terms as well as by 20 and 25 terms.

The use of formulas given in appendices 1 and 2 appreciably saves time for numerical calculation and makes it possible to obtain the matrix elements with high accuracy. By examining the symmetry of $\hat{I}$ and $\hat{J}$ given by equation (A.30), we find the calculated matrix elements to be exact within accuracy of 10^{-11} for equation (5.3) and 10^{-5} for equation (6.8), respectively. The QR transformation (cf. Francis 1961) of a matrix of Hessenberg form is used in solving eigenequations. This device also saves much time for computation. Hereinafter, we denote the number of terms in the expansion by n_t, and the dimensionless frequency $\hat{\omega}$ by ω. The real and imaginary parts of ω are denoted by ω_R and ω_I, respectively. Further, the words "eigenvalue" and "eigenmode" are used without rigorous distinction, so long as there is no room for confusion between these two concepts.

Eigenvalues generally depend on the value of n_t, and they do not always converge rapidly to certain values. There are, however, some eigenvalues which appear to converge rapidly to certain values when n_t is increased. For the equilibrium models with $0.05 \lesssim \varepsilon \lesssim 0.54$, these are *unstable* eigenmodes, the eigenvalue of which scarcely varies even if the value of n_t is changed. These eigenmodes are referred to as *B-modes*. As for *stable* eigenmodes, there is a pair of eigenmodes, the eigenvalue of which scarcely varies even if the value of n_t is changed, for the models with $0.0 \leqq \varepsilon \lesssim 0.3$. They are referred to as *S-modes*. All

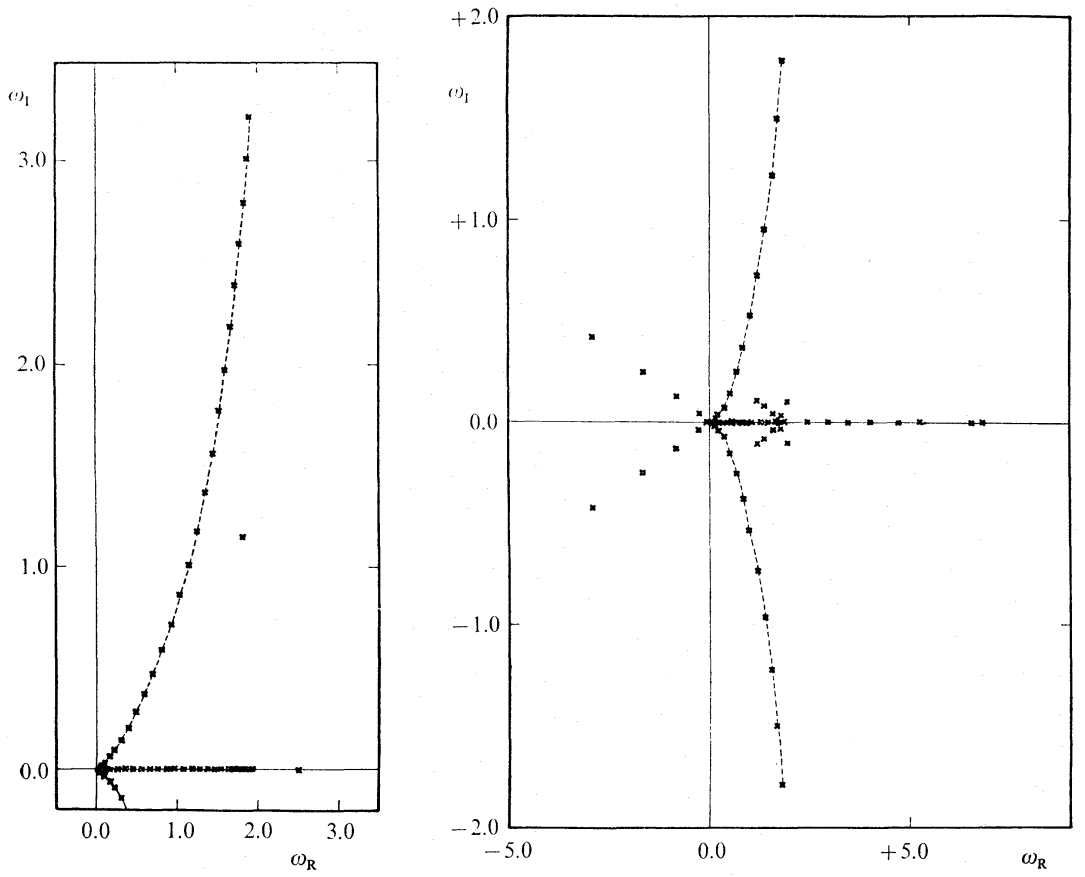

(a) $\varepsilon=0.05$ (b) $\varepsilon=0.10$

Fig. 2a-b. See the legend on the next page.

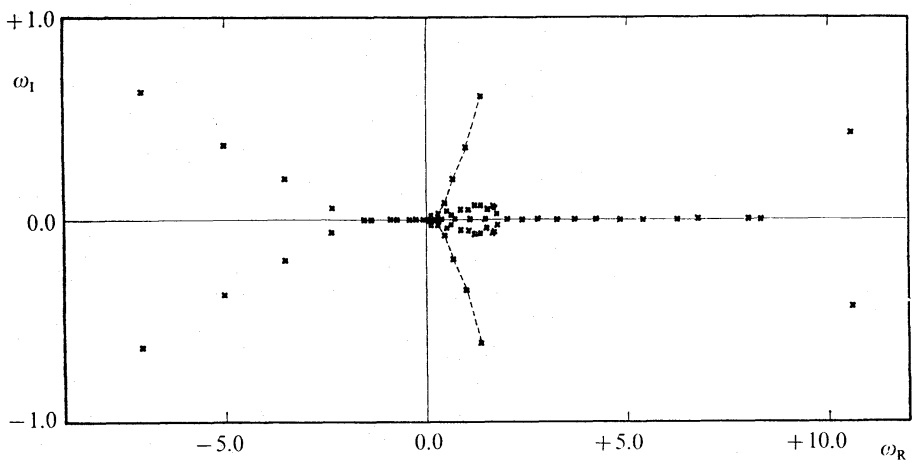

(c) $\varepsilon=0.20$

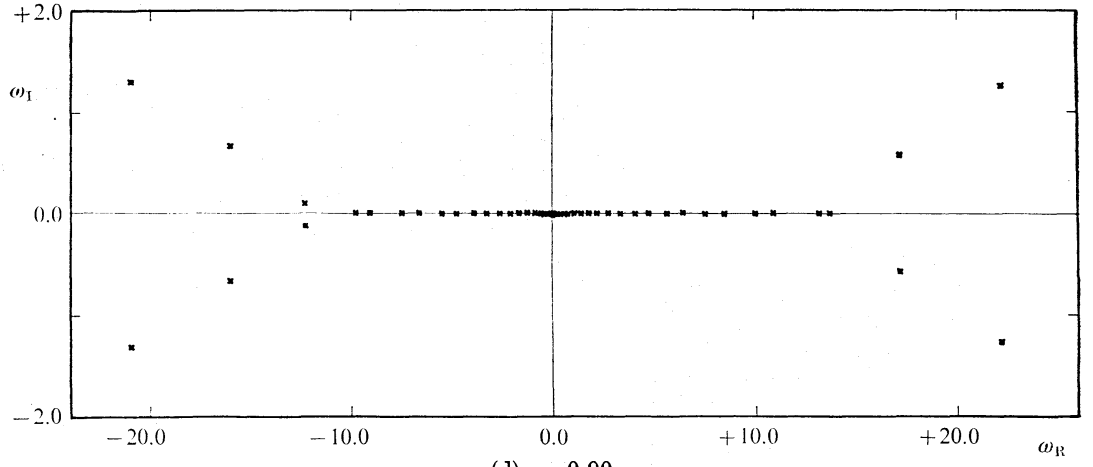

(d) $\varepsilon=0.90$

Fig. 2. Distribution of eigenvalues on the complex ω-plane in the non-axisymmetric case, $m=2$, for four disk models. The number of terms in the expansion, n_t, is 25 in all cases. Note that the scales of the ordinate and the abscissa are different. In figures 2a–c, B-modes constitute a pair of curved sequences (dashed lines) which extend to the right from the vicinity of the origin.

of the S-modes are axisymmetric. We regard B-modes and S-modes as reliable eigenmodes from the viewpoint of numerical analysis.

A general image of eigenvalue spectra for the present model family is obtained from figures 2a–d which show four typical examples of the distribution of eigenvalues on the complex ω-plane in the case $m=2$. The distribution for other values of $m(\neq 0, 2)$ are similar to those for $m=2$. As for the axisymmetric case, $m=0$, eigenvalue spectra are given in figures 3a–d. There are axisymmetric modes on the ω_I-axis when $0.0 \leqq \varepsilon \lesssim 0.05$ (see figure 3a). They are not, however, regarded as B-modes because their eigenvalues depend considerably on the value of n_t. It is noted that B-modes always constitute a pair of sequences which extend from the vicinity of the origin upward and downward, respectively (see the dashed lines in figures 2a–c and figures 3b and 3c). We refer to the pair of sequences as a *branch*.

In figure 2a, all stable eigenmodes except one are located in the interval, $0.0 \lesssim \omega_R \lesssim 2.0$, on the ω_R-axis. The number of eigenmodes in the interval increases

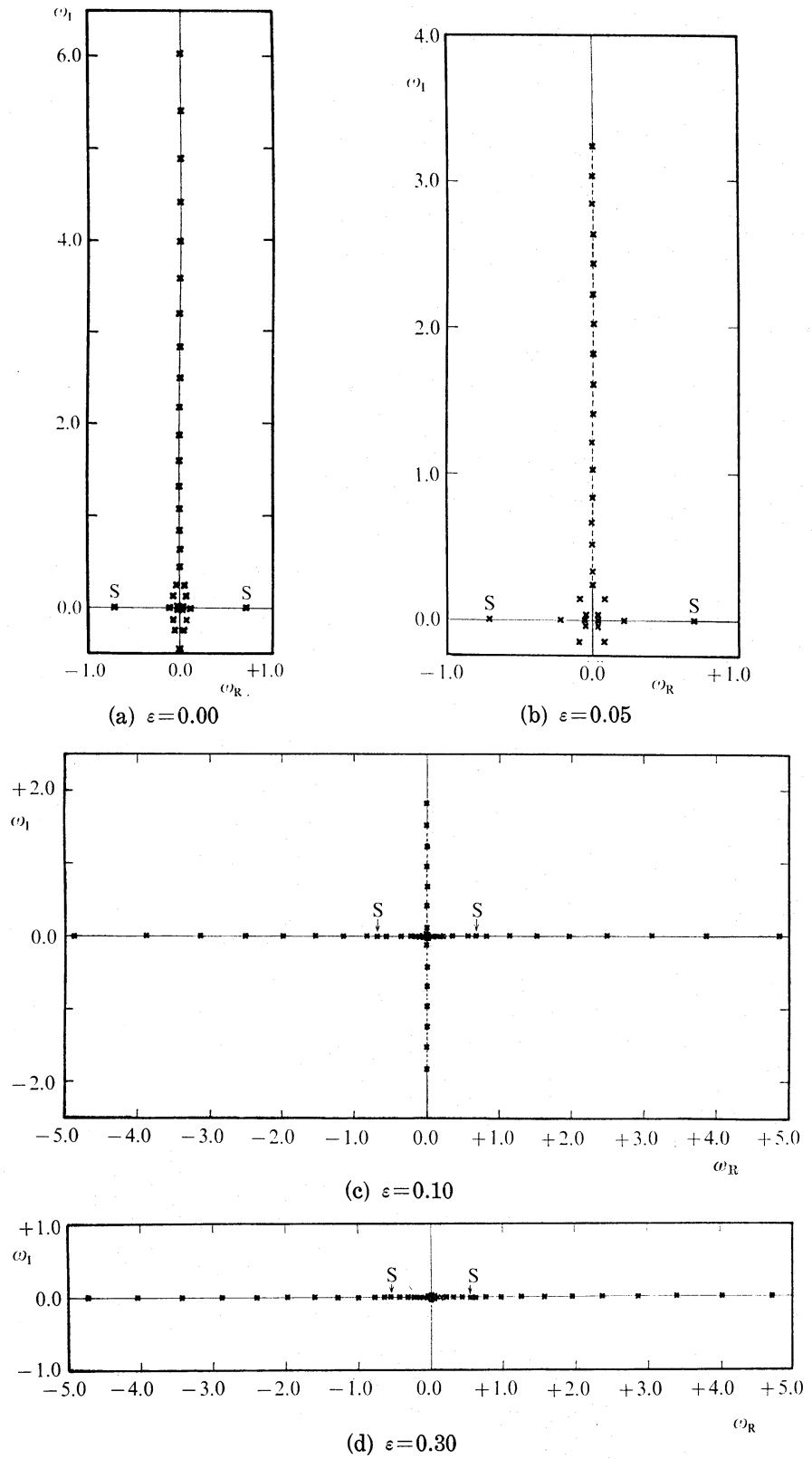

Fig. 3. Distribution of eigenvalues on the complex ω-plane in the axisymmetric case, $m=0$, for four disk models. The number n_t is 25 in all cases. S-modes are indicated by the letter "S." In figure 3d, there are twelve real eigenvalues outside the displayed region. In figures 3b and 3c, B-modes constitute a pair of straight sequences (dashed lines on the ω_I-axis).

as the number n_t increases. This fact, together with the ill convergence of stable eigenmodes, may suggest that there is a continuous spectrum of eigenvalues. We do not discuss these stable eigenmodes further because reliable data are not available.

In section 8 we confine ourselves to B-modes, and in section 9 to S-modes. This restriction does not reduce the significance of the present study for the following two reasons. (1) Mathematically speaking, in the linear theory, any obtained mode satisfies the equations of motion and of continuity independently of the other modes. Therefore, the rapid convergence of an eigenmode shows its validity, even if the convergence is doubtful for the other modes. (2) Physically speaking, we should pay attention to unstable modes with large growth rate such as B-modes rather than stable or nearly stable ones, because those highly unstable modes will play very important roles in the early stage of the evolution of galactic disturbances, even if they can be assumed to be small in amplitude initially.

Unstable eigenvalues are obtained in a conjugate pair and the property of a given eigenmode can be derived from that of the conjugate counterpart [see, for details, expressions (5.14) and the following explanation]. Therefore we consider only eigenmodes growing with time.

8. *Branches and B-modes*

In this section, we investigate the properties of eigenvalues and eigenfunctions of B-modes.

8.1. *Eigenvalues of B-modes*

We name growing B-modes further as follows for convenience. Let us fix m. The j-th unstable mode on the branch is referred to as *$B(m, j)$-mode*, regardless of the value of ε. For example, B(2, 3)-mode is the third unstable B-mode for $m=2$. We simply use the word "B-mode," if we are not interested in the particular values of m and j.

In tables 1a–f, some properties of B-modes are listed for six values of ε. Columns (1) and (2) give m, the azimuthal wavenumber, and j, the order of the growth rate, respectively. The oscillation frequency ω_R, the growth rate ω_I, and the pattern angular velocity $\omega_p(=\omega_R/m)$ are given in columns (3), (5), and (7), respectively. Columns (4) and (6) give two quantities $\Delta\omega_R$ and $\Delta\omega_I$, respectively. They are defined by

$$\Delta\omega_R = \frac{(\omega_R)_{20} - (\omega_R)_{25}}{(\omega_R)_{25}},$$

$$\Delta\omega_I = \frac{(\omega_I)_{20} - (\omega_I)_{25}}{(\omega_I)_{25}},$$

respectively. Here $(\omega_R)_k$ and $(\omega_I)_k$ stand for the values of ω_R and ω_I calculated by the k-term expansion of disturbances, respectively. Therefore, $\Delta\omega_R$ and $\Delta\omega_I$ represent the degree of convergence of the eigenvalue; the smaller, the better. In tables 1a and 1b, only first five B-modes are listed for each m. It is clear from these tables that, for fixed ε and m, the larger the growth rate is, the more rapid the convergence is. The convergence is most rapid on the whole when ε is about 0.1. All B-modes have positive pattern angular velocities. It is

Table 1a. Eigenvalues of B-modes for $\varepsilon=0.05$ ($n_t=25$).

m (1)	j (2)	$(\omega_R)_{25}$ (3)	$\Delta\omega_R$ (4)	$(\omega_I)_{25}$ (5)	$\Delta\omega_I$ (6)	ω_p (7)
0	1	0.0	—	3.241	−1.9E−3	—
0	2	0.0	—	3.035	−1.1E−2	—
0	3	0.0	—	2.830	−2.9E−2	—
0	4	0.0	—	2.628	−5.5E−2	—
0	5	0.0	—	2.427	−9.0E−2	—
1	1	0.959	+2.1E−2	3.235	−2.5E−2	0.959
1	2	0.939	−2.6E−3	3.029	−6.7E−3	0.939
1	3	0.920	+9.4E−2	2.813	−7.4E−2	0.920
1	4	0.896	−5.2E−2	2.616	−3.2E−2	0.896
1	5	0.878	+1.6E−1	2.382	−1.1E−1	0.878
2	1	1.913	−7.4E−4	3.223	−1.1E−2	0.956
2	2	1.873	−2.5E−3	3.014	−1.2E−2	0.936
2	3	1.829	−2.1E−3	2.805	−4.3E−2	0.914
2	4	1.782	−7.6E−3	2.599	−4.4E−2	0.891
2	5	1.729	+5.7E−3	2.389	−9.4E−2	0.864
3	1	2.857	−2.2E−3	3.202	−4.8E−3	0.952
3	2	2.796	−4.6E−3	2.990	−9.3E−3	0.932
3	3	2.730	−9.7E−3	2.781	−2.6E−2	0.910
3	4	2.658	−1.5E−2	2.574	−3.9E−2	0.886
3	5	2.578	−2.0E−2	2.369	−7.0E−2	0.859
4	1	3.788	−1.6E−3	3.172	−1.6E−3	0.947
4	2	3.704	−4.5E−3	2.956	−4.8E−3	0.926
4	3	3.614	−1.0E−2	2.743	−1.4E−2	0.904
4	4	3.516	−1.7E−2	2.534	−2.7E−2	0.879
4	5	3.410	−2.7E−2	2.329	−5.0E−2	0.852

Table 1b. Eigenvalues of B-modes for $\varepsilon=0.10$ ($n_t=25$).

m (1)	j (2)	$(\omega_R)_{25}$ (3)	$\Delta\omega_R$ (4)	$(\omega_I)_{25}$ (5)	$\Delta\omega_I$ (6)	ω_p (7)
0	1	0.0	—	1.820	<1.0E−9	—
0	2	0.0	—	1.523	<1.0E−9	—
0	3	0.0	—	1.233	+8.4E−9	—
0	4	0.0	—	0.951	−2.8E−7	—
0	5	0.0	—	0.680	+3.9E−6	—
1	1	0.900	−6.6E−7	1.813	+7.1E−7	0.900
1	2	0.846	+1.1E−7	1.517	+1.4E−6	0.846
1	3	0.782	+2.5E−5	1.230	+2.8E−5	0.782
1	4	0.707	+8.3E−5	0.955	+2.0E−5	0.707
1	5	0.619	+8.5E−4	0.696	−4.5E−4	0.619
2	1	1.781	+1.7E−6	1.793	+2.8E−9	0.891
2	2	1.671	+7.7E−6	1.499	−4.4E−6	0.836
2	3	1.542	+4.1E−5	1.219	−8.1E−5	0.771
2	4	1.392	−6.0E−5	0.959	−4.8E−4	0.696
2	5	1.221	−1.4E−3	0.726	−1.2E−3	0.611
3	1	2.627	−9.9E−8	1.752	−3.2E−6	0.876
3	2	2.456	−9.2E−6	1.454	−2.7E−5	0.819
3	3	2.258	−1.3E−4	1.174	−1.3E−4	0.753
3	4	2.036	−7.6E−4	0.916	+3.8E−4	0.679
3	5	1.797	−1.6E−3	0.689	+7.0E−3	0.599
4	1	3.430	−2.8E−6	1.680	−2.3E−7	0.857
4	2	3.194	−3.1E−5	1.372	+3.2E−5	0.798
4	3	2.929	−1.6E−4	1.085	+6.1E−4	0.732
4	4	2.641	+5.1E−6	0.829	+4.8E−3	0.660
4	5	2.338	+3.3E−3	0.613	+1.8E−2	0.584

Table 1c. Eigenvalues of B-modes for $\varepsilon=0.15$ ($n_t=25$).

m (1)	j (2)	$(\omega_R)_{25}$ (3)	$\Delta\omega_R$ (4)	$(\omega_I)_{25}$ (5)	$\Delta\omega_I$ (6)	ω_p (7)
0	1	0.0	—	1.068	<1.0E−9	—
0	2	0.0	—	0.686	−2.2E−7	—
0	3	0.0	—	0.297	−8.1E−5	—
1	1	0.820	−1.1E−5	1.071	+4.4E−6	0.820
1	2	0.704	+2.7E−5	0.706	+4.8E−5	0.704
1	3	0.544	+1.0E−3	0.372	−3.9E−3	0.544
1	4	0.334	−1.5E−4	0.130	+2.1E−2	0.334
2	1	1.599	+3.6E−6	1.067	+2.7E−5	0.799
2	2	1.367	+1.8E−4	0.737	−7.6E−5	0.683
2	3	1.093	−9.9E−4	0.475	−3.0E−3	0.546
2	4	0.827	−2.6E−3	0.302	+8.3E−3	0.414
2	5	0.613	+4.4E−3	0.177	+3.9E−2	0.306
2	6	0.415	+7.1E−2	0.081	−1.0E−1	0.207
3	1	2.315	+2.5E−5	1.016	+5.7E−6	0.772
3	2	1.983	+5.2E−5	0.693	−8.2E−4	0.661
3	3	1.631	−2.0E−3	0.444	−4.7E−3	0.544
3	4	1.290	−1.8E−3	0.270	+3.6E−2	0.430
3	5	1.003	−9.3E−4	0.170	+2.9E−2	0.334
3	6	0.770	−2.0E−2	0.094	+2.2E−1	0.257
4	1	2.969	+7.6E−6	0.902	−1.0E−4	0.742
4	2	2.541	+1.6E−4	0.585	−6.2E−4	0.635
4	3	2.116	−7.9E−3	0.363	−7.1E−3	0.529
4	4	1.701	+1.1E−2	0.214	+1.5E−1	0.425
4	5	1.379	+4.9E−3	0.159	−2.5E−1	0.345
4	6	1.121	−5.2E−2	0.089	+9.2E−2	0.280

Table 1d. Eigenvalues of B-modes for $\varepsilon=0.20$ ($n_t=25$).

m (1)	j (2)	$(\omega_R)_{25}$ (3)	$\Delta\omega_R$ (4)	$(\omega_I)_{25}$ (5)	$\Delta\omega_I$ (6)	ω_p (7)
0	1	0.0	—	0.494	−5.8E−7	—
1	1	0.708	+1.8E−4	0.543	+4.9E−4	0.708
1	2	0.432	−4.7E−3	0.157	+6.5E−3	0.432
2	1	1.353	+2.4E−4	0.610	+1.0E−4	0.677
2	2	0.982	−1.3E−3	0.350	−3.4E−3	0.491
2	3	0.688	−3.7E−3	0.205	+1.5E−2	0.344
2	4	0.448	+5.0E−2	0.081	+3.9E−2	0.224
3	1	1.947	+6.4E−5	0.571	−5.0E−4	0.649
3	2	1.498	−1.1E−4	0.316	−1.5E−2	0.499
3	3	1.097	−1.3E−3	0.172	+2.3E−2	0.366
3	4	0.809	−1.8E−2	0.081	+9.5E−2	0.270
4	1	2.463	−1.2E−4	0.434	+5.8E−3	0.616
4	2	1.932	−1.7E−2	0.218	−1.0E−1	0.483
4	3	1.452	+1.6E−2	0.129	+1.2E−1	0.363
4	4	1.147	−4.1E−2	0.077	−4.8E−1	0.287

Table 1e. Eigenvalues of B-modes for $\varepsilon=0.25$ ($n_t=25$).

m (1)	j (2)	$(\omega_R)_{25}$ (3)	$\Delta\omega_R$ (4)	$(\omega_I)_{25}$ (5)	$\Delta\omega_I$ (6)	ω_p (7)
2	1	1.068	+8.2E−4	0.357	+2.0E−3	0.534
2	2	0.702	+2.2E−3	0.198	−5.0E−3	0.351
2	3	0.427	−3.4E−2	0.082	−7.0E−2	0.213
3	1	1.593	+1.5E−3	0.321	−2.7E−3	0.531
3	2	1.113	+1.7E−3	0.152	+6.1E−3	0.371
3	3	0.717	+3.4E−2	0.046	−4.2E−2	0.239
4	1	1.992	−1.5E−2	0.150	+3.9E−2	0.498
4	2	1.447	+2.0E−2	0.086	+1.1E−1	0.362

Table 1f. Eigenvalues of B-modes for $\varepsilon=0.30$ ($n_t=25$).

m (1)	j (2)	$(\omega_R)_{25}$ (3)	$\Delta\omega_R$ (4)	$(\omega_I)_{25}$ (5)	$\Delta\omega_I$ (6)	ω_p (7)
2	1	0.838	−1.6E−3	0.248	−5.5E−3	0.419
2	2	0.505	+1.9E−2	0.101	+7.9E−2	0.253
3	1	1.291	+8.4E−4	0.162	−8.1E−2	0.430
4	1	1.557	−5.1E−3	0.069	+1.3E−1	0.389

also noted that the pattern angular velocities of B(m, 1)-modes for the same value of ε depend little on the value of m.

The effect of the internal energy, the amount of which is given by ε, on the growth rate of B-modes is clear from figures 4a–e, 5a, and 5b, and is summarized as follows:

(8, i) The growth rate of each B-mode decreases as ε increases (see figures 4 and 5b). Axisymmetric and non-axisymmetric B-modes are completely stabilized when ε reaches 0.24 and 0.54, respectively (see figure 5a).

(8, ii) The growth rates of B(m, 1)-modes depend little on the value of m, when $0.05\lesssim\varepsilon\lesssim0.15$. For larger ε, B(2, 1)-mode is most unstable (see figure 5a).

8.2. *Eigenfunctions of Non-axisymmetric B-modes*

Figures 6a–l show the patterns of the surface-density disturbance of B(2, 1)-, B(2, 2)-, and B(2,3)-modes. Each pattern rotates in the same direction as the equilibrium models in the non-rotating coordinate system, since ω_p is positive. There are two points of view in studying the properties of density patterns. (a) One is to investigate *how the pattern of each B-mode varies with ε, that is, the "hotness" of the equilibrium model.* (b) The other is to investigate *how the patterns of B-modes depend on the value of j, that is, the degree of instability, in the same equilibrium model.*

The properties of density patterns are summarized in the following statements which are also valid for the other values of m(=1, 3, and 4).

Figures 6 show that:

(8, iii) Each B-mode has a trailing spiral pattern with a pair of peaks near the center, regardless of the values of ε and j.

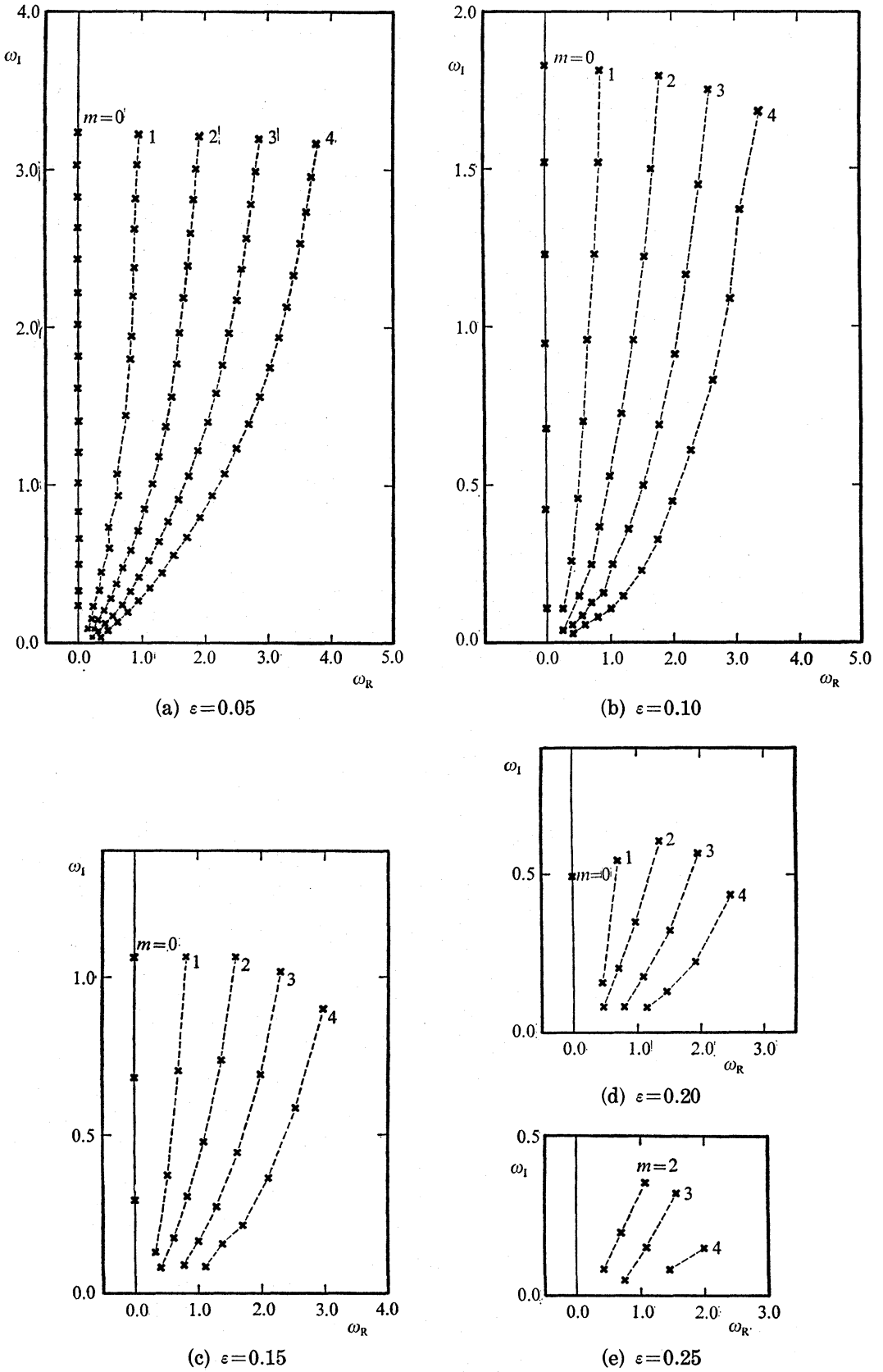

Fig. 4. Distribution of eigenvalues of growing B-modes with $0 \leqq m \leqq 4$ for five disk models. The number n_t is 25. Note that the scales of the axes are different.

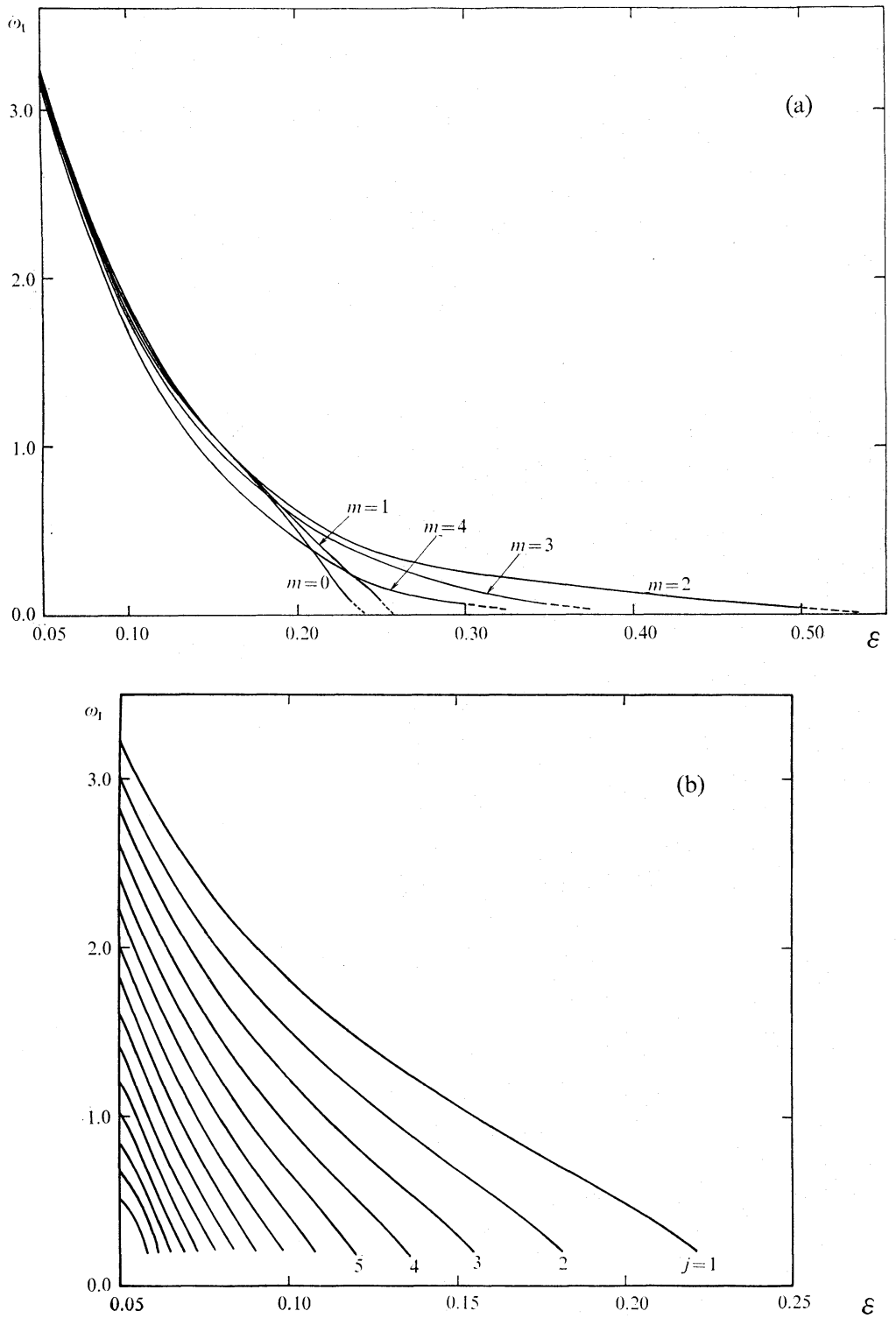

Fig. 5. (a) The growth rate of B(m, 1)-mode plotted against ε. (b) The growth rate of B(0, j)-mode plotted against ε. The number n_t is 25 in both figures. The dependence of ω_I on ε is not investigated in detail when ω_I is small.

From the viewpoint (a), we find that:

(8, iv) Spiral arms become loosely wound and inconspicuous as ε increases. Instead, a bar-like structure, which is composed of voluminous peaks and the equi-

librium density distribution, appears in the pattern of B(2, 1)-mode for large ε (see figure 6d).

(8, v) The undulation of the amplitude of disturbance along the spiral arms becomes less conspicuous as ε increases.

(8, vi) The disturbed region extends gradually as ε increases.

From the viewpoint (b) (see, for example, figures 6b, 6f, and 6j), we find that:

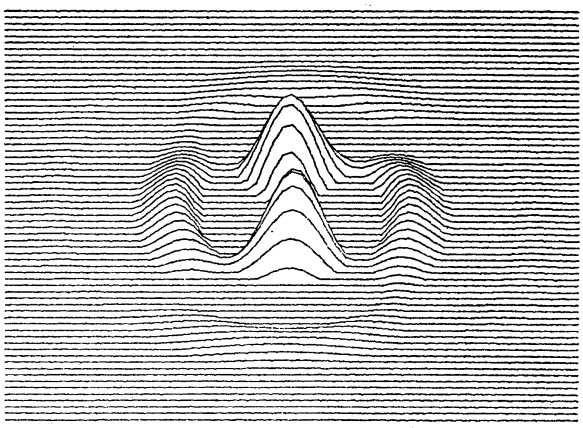

(a) B(2, 1)-mode, $\varepsilon=0.05$, $\omega=1.913+3.223i$, $R=0.5$

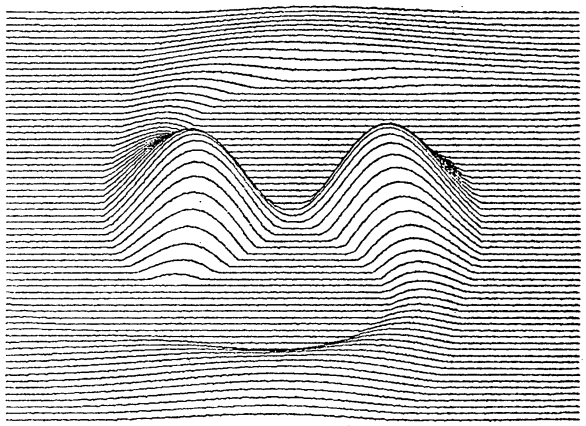

(b) B(2, 1)-mode, $\varepsilon=0.1$, $\omega=1.781+1.793i$, $R=0.5$

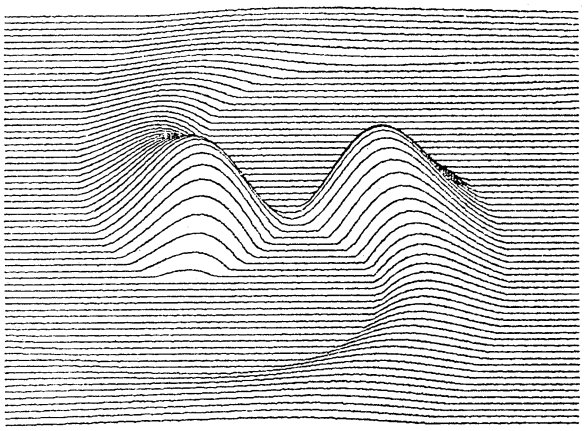

(c) B(2, 1)-mode, $\varepsilon=0.2$, $\omega=1.353+0.610i$, $R=1.0$

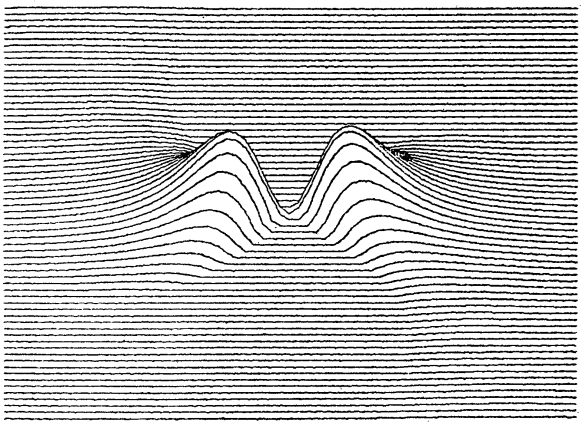

(d) B(2, 1)-mode, $\varepsilon=0.5$, $\omega=0.333+0.034i$, $R=3.0$

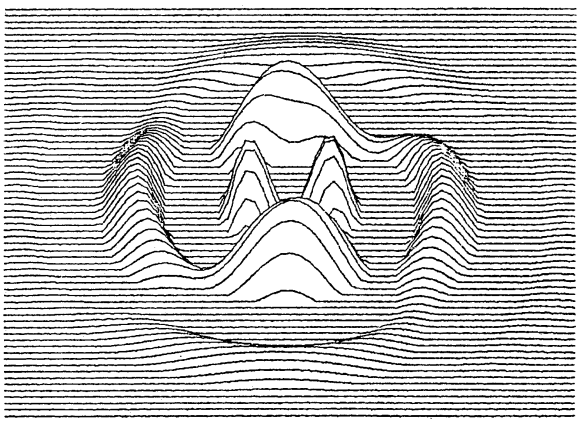

(e) B(2, 2)-mode, $\varepsilon=0.05$, $\omega=1.873+3.014i$, $R=0.5$

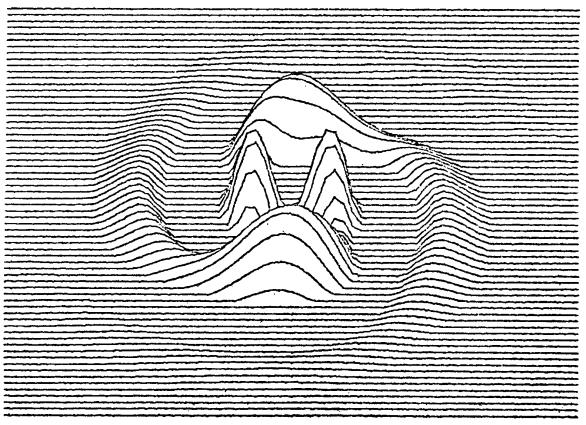

(f) B(2, 2)-mode, $\varepsilon=0.1$, $\omega=1.671+1.499i$, $R=1.0$

Fig. 6a–f. See the legend on the next page.

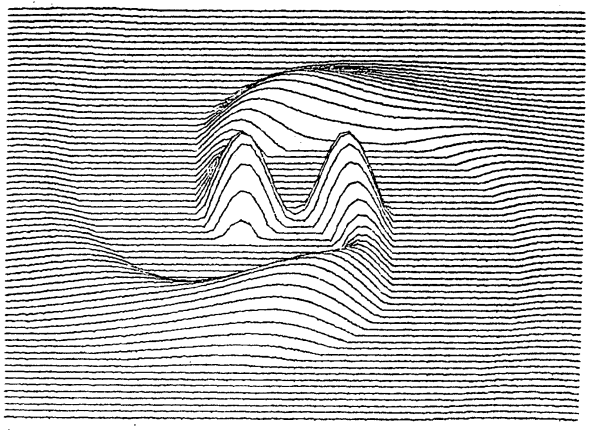

(g) B(2, 2)-mode, $\varepsilon=0.2$, $\omega=0.982+0.350i$, $R=1.5$

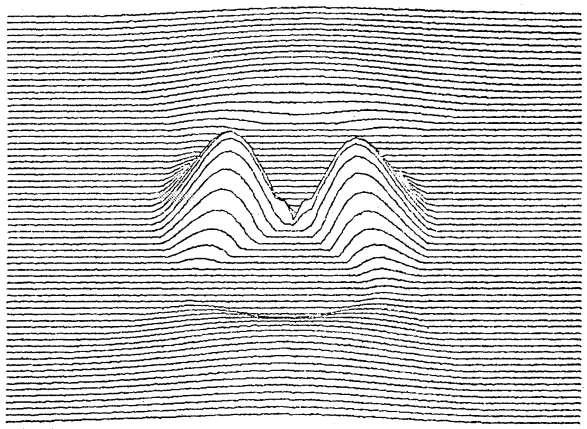

(h) B(2, 2)-mode, $\varepsilon=0\ 375$, $\omega=0.294+0.021i$, $R=2.0$

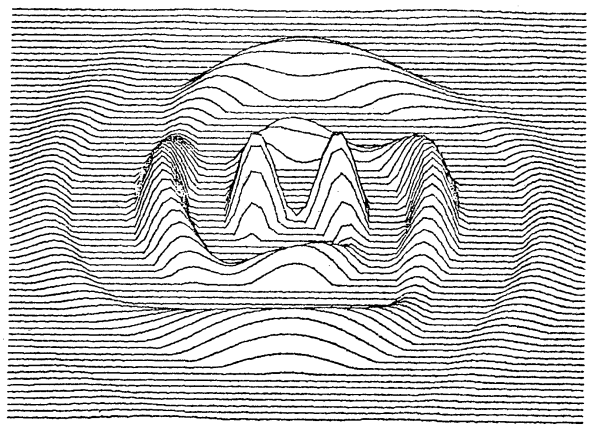

(i) B(2, 3)-mode, $\varepsilon=0.05$, $\omega=1.829+2.805i$, $R=0.5$

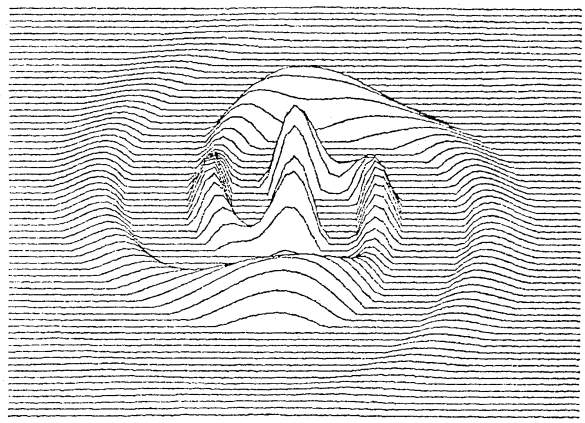

(j) B(2, 3)-mode, $\varepsilon=0.1$, $\omega=1.542+1.219i$, $R=1.0$

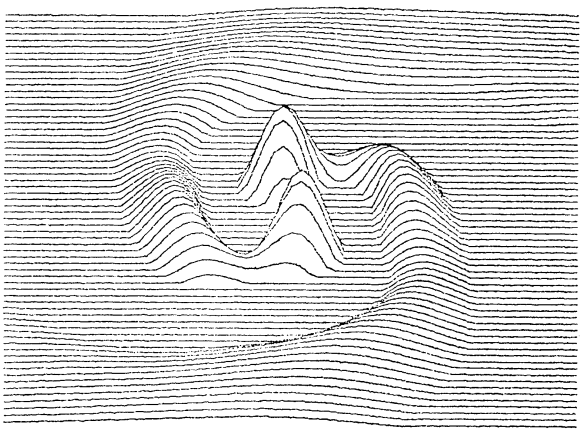

(k) B(2, 3)-mode, $\varepsilon=0.2$, $\omega=0.688+0.205i$, $R=1.5$

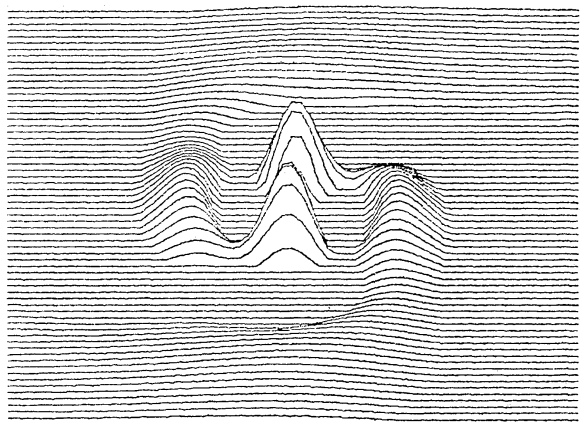

(l) B(2, 3)-mode, $\varepsilon=0.25$, $\omega=0.427+0.082i$, $R=2.0$

Fig. 6. A bird's-eye view (from the infinity) of the patterns of surface-density disturbances of B(2, 1)-, B(2, 2)-, and B(2, 3)-modes. Line of sight is inclined to the plane of the disk by 45°. R stands for the radius of the circle inscribed in the displayed square region of the disk. Only the positive part of disturbances at a certain instant of an oscillation period is plotted vertically from the plane of the disk. The vertical scale is arbitrary. The number n_t is 25.

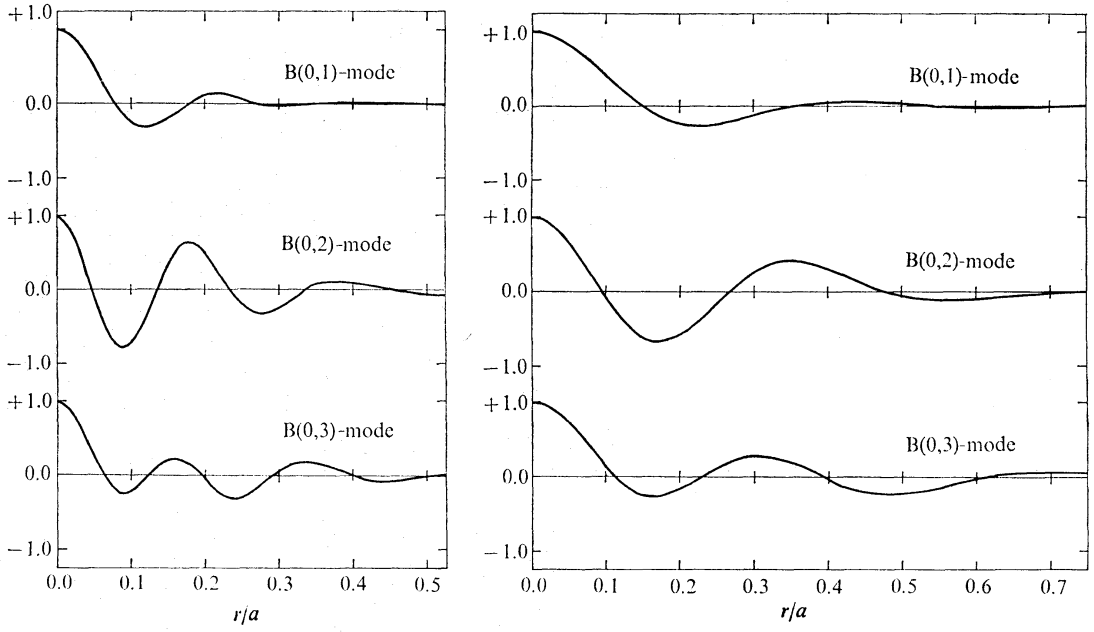

(a) $\varepsilon=0.05$ (b) $\varepsilon=0.10$

Fig. 7. The patterns of surface-density disturbances of B(0, 1)-, B(0, 2)-, and B(0,3)-modes. The amplitude of each disturbance is normalized to 1.0 at $r=0.0$. The number n_t is 25.

Table 2. Eigenvalue of S-mode ($n_t=25$).

ε (1)	$(\omega_R)_{25}$ (2)	$\Delta\omega_R$ (3)
0.0.....	0.714	+7.1E−8
0.1.....	0.677	+1.1E−5
0.2.....	0.641	−7.9E−4
0.3.....	0.632	−1.9E−2

(8, vii) Spiral arms become tightly wound and well developed (long and eminent) as j increases.
(8, viii) The undulation of the amplitude of disturbance along the spiral arms becomes more conspicuous as j increases.
(8, ix) The disturbed region extends as j increases.

8.3. *Eigenfunctions of Axisymmetric B-modes*

Since all density patterns are of axisymmetric annular shape in this case, we have only to describe their variation with respect to r, the distance from the center. Figure 7 shows the patterns of B(0, 1)-, B(0, 2)-, and B(0, 3)-modes. We first observe the variation of pattern from the viewpoint (a).
(8, x) As ε increases, the pattern is lengthened radially: that is, the radial "wavelength" becomes larger and the disturbed region extends.

From the viewpoint (b), we see that:
(8, xi) The radial wavelength becomes shorter and the disturbed region extends as j increases.

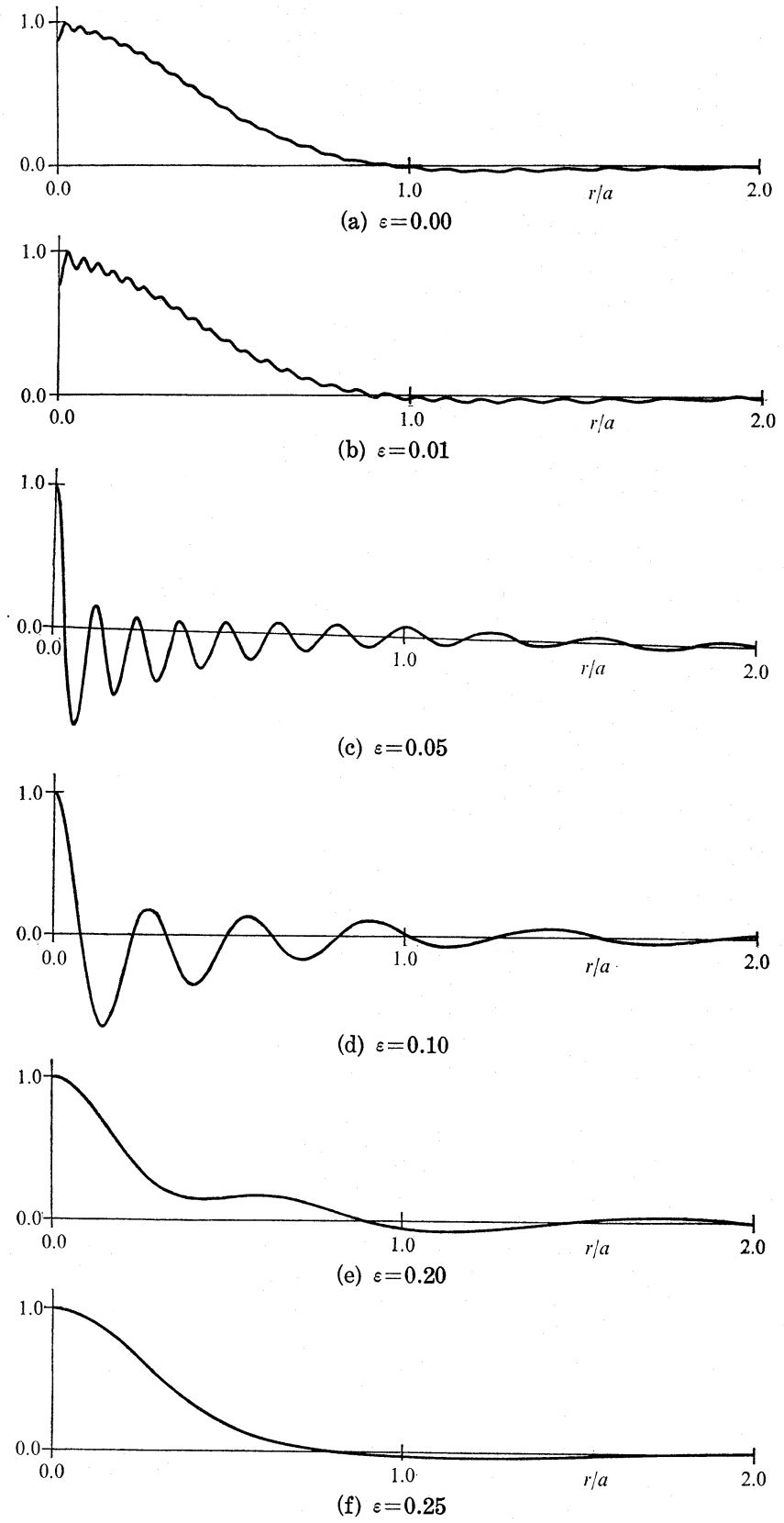

Fig. 8. The pattern of surface-density disturbance of S-mode for six disk models. The amplitude of disturbance is normalized to 1.0 at $r=0.0$. The number n_t is 75 for all figures.

9. *S-modes in the Axisymmetric Case*

The eigenvalues of two S-modes have equal absolute values but opposite signs, and their eigenfunctions μ' are the same. Therefore we consider only the S-mode with the positive eigenvalue. The eigenvalue and its accuracy are given in columns (2) and (3) of table 2. Column (1) gives the value of ε. The convergence becomes worse as ε increases. The S-mode disappears when ε exceeds about 0.3. The density pattern of the S-mode is shown in figures 8a–f. We can see the following properties from table 2 and figure 8.

(9, i) The eigenvalue remains almost the same (about 0.7), even if ε increases from 0.0 to 0.3.

(9, ii) When ε is zero, the amplitude of density disturbance diminishes slowly to zero with increasing r/a (see figure 8a). As ε increases, the pattern begins to ripple and to exhibit a short-wave structure (see figures 8b and 8c). As ε increases further, the pattern begins to be of long-wave structure again (see figures 8d–f).

10. *Discussion and Concluding Remarks*

Erickson (1974) investigated the global stability of the "gaussian model" constructed by Toomre (1963) which is more centrally concentrated than the present models. In order to simulate the effects of stellar random motions, he introduced "modified gravity" instead of gaseous pressure. He obtained eigenequations by the spline approximation, not by means of a set of orthogonal functions. Although the present analysis and his analysis are different in these respects, there are some results common to both. In the non-axisymmetric case, we see a correspondence between figure 2b or 2c in the present paper and figure 20 in Erickson's (1974) paper. The branch corresponds to what he called "line." Investigating the eigenfunctions of modes of the "line," he found that their density patterns are open trailing spirals. Moreover he found a tendency similar to the one given in (8, vii), that is, the winding of arms becomes tight as the growth rate decreases. As for the axisymmetric case, he found discrete unstable modes (U-modes in *his* notation) and discrete stable modes (S-modes in *his* notation), when the disk is sufficiently cold. We may suppose that the S-mode in the present paper corresponds to his S1-mode, and axisymmetric B-modes to his U-modes. In contrast to these remarkable similarities, there are of course a few differences between the present results and his. For example, in the non-axisymmetric case, he found a number of discrete stable eigenmodes not existing in the present models. In the axisymmetric case, he found discrete stable modes (S2 and S3) in addition to the S1-mode.

According to the present analysis, the necessary stability condition for the disk is that $\varepsilon \gtrsim 0.54$. This condition is compatible with Iye's (1978), $\varepsilon \gtrsim 0.5$. However, it is weaker than the condition $t \lesssim 0.14$ obtained by Ostriker and Peebles (1973) which is found to be equivalent to the condition $\varepsilon \gtrsim 0.72$ by equation (3.20). At any rate, we need a considerably large amount of total internal energy in order to stabilize disks.

The singularity at the edge of finite disks is removed to infinity in the present analysis since we take the infinite disk models. There is still a problem about the functional forms at infinity. Expansions (4.15), (5.1), and (6.2) cannot strictly satisfy the equations of continuity and of motion at infinity. This

is because μ_0 and Ω approach zero in the forms r^{-3} and $r^{-3/2}$, respectively, as r tends to infinity, whereas μ' and ψ' are expanded in the particular forms (4.1) and (4.2). Therefore the validity of the present analysis may be in doubt. It is however supposed that the application of expansions (4.15), (5.1), and (6.2) is justified for the following reasons: (1) As for μ' and ψ', expressions (4.1) and (4.2) give an exact solution of linearized Poisson's equation, even if their completeness as a functional set is still open to question. The gravitational force, being a long-range force, plays an essential role in the dynamics of self-gravitating systems. Therefore, it is desirable from the physical as well as the mathematical point of view to solve Poisson's equation exactly. (2) As for u' and v', in the case $m=0$, whatever form of expansions of u' and v' may be used, it does not affect at least eigenvalues and eigenvectors $\boldsymbol{a}$, since they are obtained by equation (6.8), in which u' and v' are eliminated. (3) Eigenvalues of non-axisymmetric B-modes calculated by using expansions (4.15) and (5.1) seem to be compatible with those of axisymmetric B-modes obtained by equation (6.8). In fact, the eigenvalue of B(0, j)-mode is located on the ω-plane, as if it were obtained by extrapolation from the other B(m, j)-modes for $m=1$, 2, 3, and 4 (see figures 4a–d). This fact partially shows the validity of the expansions of u' and v' given in equations (5.1) at least for B-modes. (4) Another form of expansions obtained by multiplying u' and v' in equations (5.1) by a factor $[(1-\xi)/2]^{3/4}$ gives the same eigenvalues and eigenvectors at least for B-modes with large growth rates. This suggests the existence of eigenmodes not affected by the functional forms of u' and v' at infinity ($\xi=1$). The special forms given in equations (5.1) are sufficient for such eigenmodes.

From the observational point of view, it is interesting that two-armed B(2, 1)-mode is not especially unstable compared with the other B(m, 1)-modes [see (8, ii)]. This suggests that observed patterns of spiral galaxies can be interpreted as a superposition of several eigenmodes with different number of arms. Kalnajs (1975) has analyzed the distribution of H II regions in M31 and has decomposed it into one-armed and two-armed patterns. Similar study of other galaxies is desirable. When we interpret such observational results by the present theory, we should pay attention to the following points. (1) The theory, being linear, is applicable only to small amplitude disturbances whereas density disturbances in actual spiral galaxies cannot be assumed to be of small amplitude in general. (2) Spiral structure usually observed is not a density pattern, but a luminosity pattern mainly due to spiral tracers such as H II regions and OB stars.

As for two-armed spirals, open trailing patterns suggesting late-type galaxies (Sc or SBc) are obtained as unstable global eigenmodes in the present analysis (see figures 6). On the contrary, it turns out to be difficult to obtain reliable eigenmodes that have a tightly wound spiral pattern comparable to those observed in early-type galaxies (Sa or SBa). Moreover, leading spiral patterns such as obtained by Miyamoto (1969), Iye (1978), and Takahara (1978) are not found in the present models. Although the most unstable mode for $\varepsilon \lesssim 0.03$ gives a slight sign of a tightly wound leading spiral, we omit it as not yet established because of the ill convergence of the eigenvalue. It seems to be difficult to explain short-wave disturbances such as tightly wound spirals by the present global treatment, because short-wave terms (terms with large n) are truncated in the numerical calculation. A complementary analysis of the present models based on the local theory is in progress.

In conclusion, the following trends are confirmed concerning the global instability of Toomre's (1963) disk models with gaseous pressure with the polytropic exponent $\Gamma=4/3$:

(1) The increasing internal energy serves to stabilize the disk as is expected. There remain, however, unstable ring modes as long as $\varepsilon\lesssim 0.24$, and unstable spiral modes as long as $\varepsilon\lesssim 0.54$.

(2) Not only two-armed ($m=2$) spiral modes but also one-armed and multi-armed spiral modes as well as ring modes are expected to grow within a few rotation periods of the disk in general.

(3) Unstable spiral modes are trailing unless the disk is extremely cold ($\varepsilon\lesssim 0.05$), where the results are not certain owing to the insufficient numerical accuracy.

(4) The tightly wound spirals such as Sa or SBa are not recognized, as far as the most rapidly growing modes are concerned, but as for the less unstable modes of sufficiently cool disks, there may be modes comparable to Sa. Hotter disks have only bar-like or sectorial modes even for unstable ones.

(5) The spiral patterns are not smooth for less unstable modes of relatively cool disks. The amplitude of disturbance undulates along the spiral arms. This fact may explain the patchy structures of arms observed in actual galaxies.

(6) The patterns of unstable spiral modes propagate in the same direction as that of galactic rotation. The most rapidly growing modes for the first several azimuthal Fourier components have nearly the same pattern speed. The growth time of these modes is comparable with the period of rotation of the system.

The authors would like to express their hearty gratitude to the referees, who gave us important suggestions on the original manuscript. The authors also express their thanks to Miss K. Uzawa and Miss Y. Yao for typing the manuscript. The computational part of this work was performed on the FACOM 230/58 computer at the Tokyo Astronomical Observatory.

Appendix 1. *Recurrence Formulas for* $\hat{I}(\alpha, m; l, n)$ *and* $\hat{J}(\alpha, m; l, n)$

Throughout the present work we use the following definition of the associated Legendre functions for a real valued argument:

$$P_n^m(\xi)=\frac{(1-\xi^2)^{m/2}}{n!\,2^n}\frac{d^{n+m}}{d\xi^{n+m}}(\xi^2-1)^n\,, \tag{A.1}$$

where m, n are integers such that

$$0\leqq m\leqq n\,, \tag{A.2}$$

and ξ denotes a real value satisfying

$$-1\leqq\xi\leqq 1\,. \tag{A.3}$$

It is noted that this definition differs from that of Erdélyi et al. (1953) by a factor $(-1)^m$. In order to save space we introduce the notation

$$(2m-1)!!=\frac{(2m)!}{2^m m!}=(2m-1)(2m-3)\cdots 3\cdot 1\,. \tag{A.4}$$

We have introduced the integrated quantities $\hat{I}(\alpha, m; l, n)$ and $\hat{J}(\alpha, m; l, n)$ by equations (5.16) and (5.17), respectively. In order to obtain the recurrence formulas for them, we introduce here

$$\left.\begin{aligned} I(\alpha, m; l, n) &= \int_{-1}^{1} \left(\frac{1-\xi}{2}\right)^{\alpha} P_l^m(\xi) P_n^m(\xi) d\xi , \\ J(\alpha, m; l, n) &= \int_{-1}^{1} \left(\frac{1-\xi}{2}\right)^{\alpha} \left(\frac{1+\xi}{2}\right)^{-1} P_l^m(\xi) P_n^m(\xi) d\xi , \end{aligned}\right\} \tag{A.5}$$

for brevity. Also we define

$$\left.\begin{aligned} I'(\alpha+1, m; l, n) &= \int_{-1}^{1} \xi \left(\frac{1-\xi}{2}\right)^{\alpha} P_l^m(\xi) P_n^m(\xi) d\xi , \\ J'(\alpha+1, m; l, n) &= \int_{-1}^{1} \xi \left(\frac{1-\xi}{2}\right)^{\alpha} \left(\frac{1+\xi}{2}\right)^{-1} P_l^m(\xi) P_n^m(\xi) d\xi . \end{aligned}\right\} \tag{A.6}$$

Putting

$$\nu = \left[\frac{(n-m)!\,(2n+1)}{2\quad (n+m)!}\right]^{1/2} \left[\frac{(l-m)!\,(2l+1)}{2\quad (l+m)!}\right]^{1/2} , \tag{A.7}$$

which may be called a normalization factor for I etc., we have

$$\hat{I}(\alpha, m; l, n) = \nu I(\alpha, m; l, n) , \tag{A.8}$$

and so on. Since we have

$$\xi P_l^m(\xi) = \frac{(l-m+1)}{(2l+1)} P_{l+1}^m(\xi) + \frac{(l+m)}{(2l+1)} P_{l-1}^m(\xi) , \tag{A.9}$$

we obtain

$$\begin{aligned} I'(\alpha+1, m; l, n) = {} & \frac{(l-m+1)}{(2l+1)} I(\alpha, m; l+1, n) \\ & + \frac{(l+m)}{(2l+1)} I(\alpha, m; l-1, n) . \end{aligned} \tag{A.10}$$

Since I is symmetric with respect to l and n, changing the roles of l and n and replacing $n+1$ by n, we obtain, for $m \geqq 0$,

$$\begin{aligned} I(\alpha, m; l, n) = {} & \frac{2n-1}{n-m} I'(\alpha+1, m; l, n-1) \\ & - \frac{n-1+m}{n-m} I(\alpha, m; l, n-2) . \end{aligned} \tag{A.11}$$

It is noted that we have

$$I(\alpha, m; l', n') = 0 , \quad \text{for} \quad l' < m \quad \text{and/or} \quad n' < m , \tag{A.12}$$

due to the vanishing of the Legendre function. Replacing n in equation (A.10) by $n-1$ and inserting the equation into the right-hand side of equation (A.11), we obtain $I(\alpha, m; l, n)$ in terms of $I(\alpha, m; l+1, n-1)$, $I(\alpha, m; l-1, n-1)$, and $I(\alpha, m; l, n-2)$. Since the sum of the third and fourth arguments does not increase by this operation, $I(\alpha, m; l, n)$ is expressed finally in terms of

$I(\alpha, m; l', m)$, where $m \leqq l' \leqq l+n-m$. It is noted that the above recurrence formulas (A.10) and (A.11) are applied to J and J' as well, since we do not use the peculiarity of the integrand except for the factors P_l^m and P_n^m.

The next step is to calculate the integrals for $n=m$. Using integration by parts, and applying

$$\frac{d}{d\xi} P_l^m(\xi) = \frac{1}{1-\xi^2}[m\xi P_l^m(\xi) - (l+m)(l-m+1)(1-\xi^2)^{1/2} P_l^{m-1}(\xi)], \tag{A.13}$$

we obtain

$$\begin{aligned} I(\alpha, m; l, m) &= (2m-1)!! \int_{-1}^{1} \left(\frac{1-\xi}{2}\right)^{\alpha} (1-\xi^2)^{m/2} P_l^m(\xi) d\xi \\ &= -\frac{(2m-1)!!\, 2(l-m+1)(l+m)}{\alpha+1} \int_{-1}^{1} \left(\frac{1-\xi}{2}\right)^{\alpha+1} (1-\xi^2)^{(m-1)/2} P_l^{m-1}(\xi) d\xi \\ &\quad + \left[-\frac{(2m-1)!!\, (1-\xi)^{\alpha+1}}{2^{\alpha} (\alpha+1)} (1-\xi^2)^{m/2} P_l^m(\xi) \right]_{-1}^{1} . \end{aligned} \tag{A.14}$$

The second term in the right-hand side is zero for $\alpha+m>-1$. Therefore

$$I(\alpha, m; l, m) = -\frac{2(l-m+1)(l+m)\,(2m-1)}{\alpha+1} I(\alpha+1, m-1; l, m-1) . \tag{A.15}$$

Replacing $\alpha+1$ by α, and $m-1$ by m, we have

$$I(\alpha, m; l, m) = -\frac{\alpha I(\alpha-1, m+1; l, m+1)}{2(l-m)(l+m+1)\,(2m+1)} . \tag{A.15'}$$

By means of successive applications of this recurrence formula, we obtain finally

$$I(\alpha, m; l, m) = \frac{(-1)^{l-m}(2m-1)!!\, 2^{m+1}\Gamma(\alpha+1)\,\Gamma(\alpha+m+1)(l+m)!}{\Gamma(\alpha+1-l+m)\Gamma(\alpha+m+l+2)(l-m)!} , \tag{A.16}$$

since we have, by evaluation of the Beta function,

$$\begin{aligned} I(\alpha-l+m, l; l, l) &= [(2l-1)!!]^2 2^{2l+1} \int_0^1 x^l (1-x)^{\alpha+m} dx \\ &= [(2l-1)!!]^2 2^{2l+1} \frac{\Gamma(l+1)\Gamma(\alpha+m+1)}{\Gamma(\alpha+l+m+2)} , \end{aligned} \tag{A.17}$$

where

$$x = (1+\xi)/2 .$$

Comparing the values of $I(\alpha, m; l, m)$ and $I(\alpha, m; l-1, m)$, and applying normalization factors, we arrive at the recurrence formula

$$\hat{I}(\alpha, m; l, m) = \frac{l-\alpha-m-1}{l+\alpha+m+1} \left[\frac{(l+m)(2l+1)}{(l-m)(2l-1)}\right]^{1/2} \times \hat{I}(\alpha, m; l-1, m) ,$$

$$\text{for} \quad \alpha+m>-1 , \quad l>m , \tag{A.18}$$

and an equation

$$\hat{I}(\alpha, m; m, m) = 2^m \left(\frac{2m+1}{\alpha+2m+1}\right)\left(\frac{2m-1}{\alpha+2m}\right) \cdots\cdots \left(\frac{3}{\alpha+m+2}\right)\left(\frac{1}{\alpha+m+1}\right) . \tag{A.19}$$

By applying normalization factors, equations (A.10) and (A.11) are rewritten, respectively, as

$$\hat{I}'(\alpha+1, m; l, n)=\left[\frac{(l+m+1)(l-m+1)}{(2l+1)(2l+3)}\right]^{1/2}\hat{I}(\alpha, m; l+1, n)$$
$$+\left[\frac{(l+m)(l-m)}{(2l+1)(2l-1)}\right]^{1/2}\hat{I}(\alpha, m; l-1, n)\ , \tag{A.20}$$

$$\hat{I}(\alpha, m; l, n)=\left[\frac{(2n+1)(2n-1)}{(n+m)(n-m)}\right]^{1/2}\hat{I}'(\alpha+1, m; l, n-1)$$
$$-\left[\frac{(n+m-1)(n-m-1)(2n+1)}{(n+m)(n-m)(2n-3)}\right]^{1/2}\hat{I}(\alpha, m; l, n-2)\ . \tag{A.21}$$

As for $J(\alpha, m; l, m)$, using the formula

$$P_l^m(\xi)=P_{l-2}^m(\xi)+(2l-1)(1-\xi^2)^{1/2}P_{l-1}^{m-1}(\xi)\ , \tag{A.22}$$

we have

$$J(\alpha, m; l, m)=J(\alpha, m; l-2, m)+4(2l-1)(2m-1)I(\alpha+1, m-1; l-1, m-1)\ . \tag{A.23}$$

Applying normalization factors, we obtain, instead of equation (A.18),

$$\hat{J}(\alpha, m; l, m)=\left[\frac{(l-m)(l-m-1)(2l+1)}{(l+m)(l+m-1)(2l-3)}\right]^{1/2}\hat{J}(\alpha, m; l-2, m)$$
$$+4\left[\frac{(2m+1)(2l+1)(2l-1)}{2m\quad(l+m)(l+m-1)}\right]^{1/2}\hat{I}(\alpha+1, m-1; l-1, m-1)\ . \tag{A.24}$$

$J(\alpha, m; m, m)$ and $J(\alpha, m; m+1, m)$ can be calculated by equation (A.16) and a Beta function formula such as equation (A.17), provided that $\alpha+m>-1$, and we have, instead of equation (A.19),

$$\hat{J}(\alpha, m; m, m)=\frac{2^m}{m}\left(\frac{2m+1}{\alpha+2m}\right)\left(\frac{2m-1}{\alpha+2m-1}\right)\cdots\cdots\left(\frac{3}{\alpha+m+1}\right) \tag{A.25}$$

and

$$\hat{J}(\alpha, m; m+1, m)=-\frac{2^m(2m+1)!!(2m+3)^{1/2}(\alpha+1)}{m}$$
$$\times\left(\frac{1}{\alpha+2m+1}\right)\left(\frac{1}{\alpha+2m}\right)\cdots\cdots\left(\frac{1}{\alpha+m+1}\right)\ . \tag{A.26}$$

Similarly to equations (A.20) and (A.21), we obtain

$$\hat{J}'(\alpha+1, m; l, n)=\left[\frac{(l+m+1)(l-m+1)}{(2l+1)\quad(2l+3)}\right]^{1/2}\hat{J}(\alpha, m; l+1, n)$$
$$+\left[\frac{(l+m)\,(l-m)}{(2l+1)(2l-1)}\right]^{1/2}\hat{J}(\alpha, m; l-1, n) \tag{A.27}$$

and

$$\hat{J}(\alpha, m; l, n)=\left[\frac{(2n+1)(2n-1)}{(n+m)(n-m)}\right]^{1/2}\hat{J}'(\alpha+1, m; l, n-1)$$
$$-\left[\frac{(n+m-1)(n-m-1)\,(2n+1)}{(n+m)\quad(n-m)\quad(2n-3)}\right]^{1/2}\hat{J}(\alpha, m; l, n-2)\ . \tag{A.28}$$

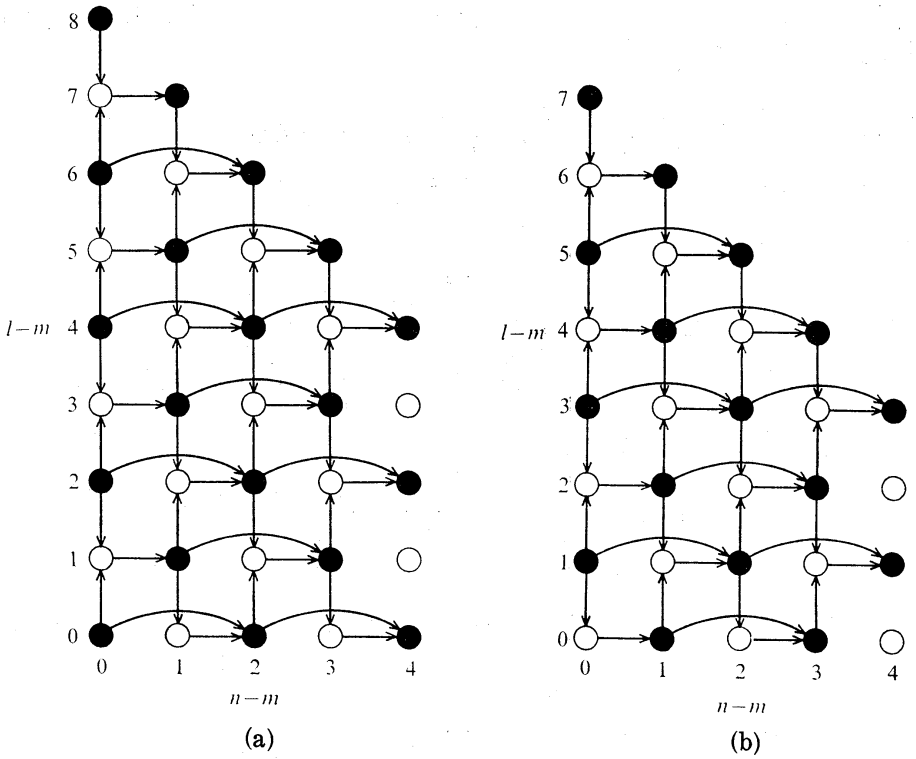

Fig. A1. A diagram for calculating $\hat{I}(\alpha, m; l, n)$ by recurrence formulas (A.20) and (A.21). Filled circles and open circles indicate $\hat{I}$ and $\hat{I}'$, respectively. Manipulations given by equations (A.20) and (A.21) are represented by vertical and horizontal arrows, respectively. Values of $\hat{I}$ at the starting line, $n-m=0$, are obtained by equations (A.18) and (A.19). Figures A1(a) and A1(b) show the whole process. These figures also indicate the process of calculation of $\hat{J}(\alpha, m; l, n)$.

Equations (A.18)–(A.21) and (A.24)–(A.28) complete the necessary recurrence formulas, provided that

$$\alpha+m>-1\,. \tag{A.29}$$

The process of calculation is shown in figure A1.

Numerical tests were performed verifying the relation

$$\hat{I}(\alpha, m; l, n)=\hat{I}(\alpha, m; n, l)\,, \tag{A.30}$$

and a similar equation for $\hat{J}$.

Appendix 2. *Evaluation of Matrix Elements Necessary for the Case* $m=0$

We consider a differentiation operator $\tilde{B}$ defined by

$$\tilde{B}f=4\left(\frac{1-\xi}{2}\right)^{1/2}\frac{d}{d\xi}\left[\left(\frac{1-\xi}{2}\right)^{1/2}\left(\frac{1+\xi}{2}\right)f\right], \tag{A.31}$$

where f is a function of ξ and expanded in terms of Legendre functions. By multiplying $\hat{P}_l$'s ($l=0, 1, 2, \cdots$) from the left on both sides of equation (A.31) and

integrating the equation from $\xi=-1$ to $\xi=1$, we obtain a matrix representation of the operator $\tilde{B}$ in the form of a matrix B given in equation (6.5). The (l, n)-element of B is given by

$$B_{l,n}=4\int_{-1}^{1}\hat{P}_l(\xi)\left(\frac{1-\xi}{2}\right)^{1/2}\frac{d}{d\xi}\left[\left(\frac{1-\xi}{2}\right)^{1/2}\left(\frac{1+\xi}{2}\right)\hat{P}_n(\xi)\right]d\xi$$
$$=-\frac{n+1}{2}\left(\frac{2n+3}{2n+1}\right)^{1/2}\delta_{l,n+1}+\frac{1}{2}\delta_{l,n}+\frac{n}{2}\left(\frac{2n-1}{2n+1}\right)^{1/2}\delta_{l,n-1}\,. \tag{A.32}$$

We begin with the evaluation of the matrix B^{-1}. From equation (A.31), we obtain $\tilde{B}^{-1}$, the inverse operator of $\tilde{B}$, as

$$\tilde{B}^{-1}f=\frac{1}{4}\left(\frac{1-\xi}{2}\right)^{-1/2}\left(\frac{1+\xi}{2}\right)^{-1}\left[\int_{-1}^{\xi}\left(\frac{1-\xi'}{2}\right)^{-1/2}f(\xi')d\xi'+\text{constant}\right]. \tag{A.33}$$

Though the integral constant in equation (A.33) can be chosen freely, we assume it to be zero in order to avoid a singularity at $\xi=-1$. Note that this choice is consistent with the adoption of expansion for u' in equations (6.2). Thus the matrix B^{-1} representing the operator $\tilde{B}^{-1}$ is obtained as

$$(B^{-1})_{l,n}=\frac{1}{4}\int_{-1}^{1}\hat{P}_l(\xi)\left(\frac{1-\xi}{2}\right)^{-1/2}\left(\frac{1+\xi}{2}\right)^{-1}\left[\int_{-1}^{\xi}\left(\frac{1-\xi'}{2}\right)^{-1/2}\hat{P}_n(\xi')d\xi'\right]d\xi\,. \tag{A.34}$$

In particular

$$(B^{-1})_{0,0}=\frac{1}{4}\int_{-1}^{1}\hat{P}_0(\xi)\left(\frac{1-\xi}{2}\right)^{-1/2}\left(\frac{1+\xi}{2}\right)^{-1}\left[\int_{-1}^{\xi}\left(\frac{1-\xi'}{2}\right)^{-1/2}\hat{P}_0(\xi')d\xi'\right]d\xi$$
$$=2\ln 2\,. \tag{A.35}$$

Now, writing explicitly the $(0, n)$-element of the equation $(B^{-1})B=E$ (unit matrix), we obtain a recurrence formula for $(B^{-1})_{0,n+1}$:

$$(B^{-1})_{0,n+1}=\frac{1}{n+1}\left(\frac{2n+1}{2n+3}\right)^{1/2}(B^{-1})_{0,n}+\frac{n}{n+1}\left(\frac{2n-1}{2n+3}\right)^{1/2}(B^{-1})_{0,n-1}$$
$$-\frac{2}{n+1}\left(\frac{2n+1}{2n+3}\right)^{1/2}\delta_{0,n}\,,\qquad \text{for}\quad n\geqq 0\,, \tag{A.36}$$

by using the explicit expression (A.32). Since the second term in the right-hand side of equation (A.36) disappears when $n=0$, this recurrence formula yields the value of $(B^{-1})_{0,n}$ for any $n\geqq 1$, starting from the value of $(B^{-1})_{0,0}$ already given by equation (A.35). Successive applications of recurrence formula (A.36) give the values of several $(B^{-1})_{0,n}$ with small n as follows:

$$(B^{-1})_{0,1}=\frac{2}{3^{1/2}}(\ln 2-1)\,,$$

$$(B^{-1})_{0,2}=\frac{2}{5^{1/2}}\left(\ln 2-1+\frac{1}{2}\right),$$

$$(B^{-1})_{0,3}=\frac{2}{7^{1/2}}\left(\ln 2-1+\frac{1}{2}-\frac{1}{3}\right),$$

and so on. From these expressions, we presume the general expression for $(B^{-1})_{0,n}$

as follows:

$$(B^{-1})_{0,n}=\frac{2}{(2n+1)^{1/2}}\left[\ln 2-\sum_{j=0}^{n-1}\frac{(-1)^j}{j+1}\right], \quad \text{for} \quad n\geqq 0\,. \tag{A.37}$$

We have used here a convention of notation

$$\sum_{j=0}^{-1} h_j=0\,, \tag{A.38}$$

in order that equation (A.37) includes the case for $n=0$. Using recurrence formula (A.36), we can prove the validity of expression (A.37) by a mathematical induction.

As for the case $l\neq 0$, writing the (l, n)-element of the equation $B(B^{-1})=E$, we obtain the recurrence formula:

$$(B^{-1})_{l+1,n}=\frac{1}{l+1}\left(\frac{2l+3}{2l+1}\right)^{1/2}[2\delta_{l,n}-(B^{-1})_{l,n}]+\frac{l}{l+1}\left(\frac{2l+3}{2l-1}\right)^{1/2}(B^{-1})_{l-1,n}\,. \tag{A.39}$$

Again successive applications of recurrence formula (A.39) give leading elements:

$$(B^{-1})_{1,n}=-2\left(\frac{3}{2n+1}\right)^{1/2}\left[\ln 2-\sum_{j=0}^{\max(0,n-1)}\frac{(-1)^j}{j+1}\right], \tag{A.40}$$

$$(B^{-1})_{2,n}=2\left(\frac{5}{2n+1}\right)^{1/2}\left[\ln 2-\sum_{j=0}^{\max(1,n-1)}\frac{(-1)^j}{j+1}\right], \tag{A.41}$$

and so on. By inspection of these equations, we presume that the general form is expressed by

$$(B^{-1})_{l,n}=2(-1)^l\left(\frac{2l+1}{2n+1}\right)^{1/2}\left[\ln 2-\sum_{j=0}^{\max(l-1,n-1)}\frac{(-1)^j}{j+1}\right], \tag{A.42}$$

where the convention given by notation (A.38) is used. The validity of the general expression (A.42) is also proven by a mathematical induction similar to the case $l=0$.

A derivation of the elements of the matrix BD is performed as follows. The operator $\tilde{D}$ represented by the matrix D in equation (6.5) is given by

$$\tilde{D}f=4\left(\frac{1}{2n+1}-\frac{\varepsilon}{3}\right)\left(\frac{1-\xi}{2}\right)^2\frac{d}{d\xi}\left[\left(\frac{1-\xi}{2}\right)^{1/2}f\right]. \tag{A.43}$$

Therefore the product of operators $\tilde{B}$ and $\tilde{D}$ is given by

$$\tilde{B}\tilde{D}f=16\left(\frac{1}{2n+1}-\frac{\varepsilon}{3}\right)\left(\frac{1-\xi}{2}\right)^{1/2}\frac{d}{d\xi}\left[\left(\frac{1-\xi}{2}\right)^{5/2}\left(\frac{1+\xi}{2}\right)\frac{d}{d\xi}\left(\frac{1-\xi}{2}\right)^{1/2}f\right]. \tag{A.44}$$

From this, we obtain the matrix BD representing the operator $\tilde{B}\tilde{D}$ as follows:

$$(BD)_{l,n}=16\left(\frac{1}{2n+1}-\frac{\varepsilon}{3}\right)\int_{-1}^{1}\hat{P}_l(\xi)\left(\frac{1-\xi}{2}\right)^{1/2}\frac{d}{d\xi}\left[\left(\frac{1-\xi}{2}\right)^{5/2}\left(\frac{1+\xi}{2}\right)\times\frac{d}{d\xi}\left(\frac{1-\xi}{2}\right)^{1/2}\hat{P}_n(\xi)\right]d\xi\,. \tag{A.45}$$

By using the recurrence formula and the differentiation formula for Legendre

functions and the relation given by

$$\frac{d}{d\xi}(1-\xi^2)\frac{d}{d\xi}P_n(\xi)=-n(n+1)P_n(\xi)\,,$$

we arrive at the final expression:

$$\begin{aligned}(BD)_{l,n}=\left(\frac{1}{2n+1}-\frac{\varepsilon}{3}\right)\Bigg[&\frac{(n+1)(2n^2+7n+3)}{(2n+1)^{1/2}(2n+3)^{1/2}}\hat{I}\left(\frac{3}{2},\,0;\,l,\,n+1\right)\\&-(2n^2+2n-1)\,\hat{I}\left(\frac{3}{2},\,0;\,l,\,n\right)\\&+\frac{n(2n^2-3n-2)}{(2n+1)^{1/2}(2n-1)^{1/2}}\hat{I}\left(\frac{3}{2},0;\,l,\,n-1\right)\Bigg],\end{aligned}\tag{A.46}$$

where we have used the notation given by equation (5.16).

Finally, we evaluate the elements of BF. The elements of the matrix F are given by

$$\begin{aligned}F_{l,n}&=(1-\varepsilon)\int_{-1}^{1}\hat{P}_l(\xi)\left(\frac{1-\xi}{2}\right)^{3/2}\left[1+3\left(\frac{1-\xi}{2}\right)\right]\hat{P}_n(\xi)d\xi\\&=(1-\varepsilon)\hat{I}\left(\frac{3}{2},\,0;\,l,\,n\right)+3(1-\varepsilon)\hat{I}\left(\frac{5}{2},\,0;\,l,\,n\right).\end{aligned}\tag{A.47}$$

Using equation (A.32), we obtain the elements of BF as follows:

$$\begin{aligned}(BF)_{l,n}=(1-\varepsilon)\Bigg\{&-\frac{l}{2}\left(\frac{2l+1}{2l-1}\right)^{1/2}\left[\hat{I}\left(\frac{3}{2},0;\,l-1,\,n\right)+3\hat{I}\left(\frac{5}{2},0;\,l-1,\,n\right)\right]\\&+\frac{1}{2}\left[\hat{I}\left(\frac{3}{2},0;\,l,\,n\right)+3\hat{I}\left(\frac{5}{2},0;\,l,\,n\right)\right]\\&+\frac{l+1}{2}\left(\frac{2l+1}{2l+3}\right)^{1/2}\left[\hat{I}\left(\frac{3}{2},0;\,l+1,\,n\right)+3\hat{I}\left(\frac{5}{2},0;\,l+1,\,n\right)\right]\Bigg\}\,.\end{aligned}\tag{A.48}$$

As a result, the matrix elements of B^{-1}, BD, and BF are expressed by equations (A.42), (A.46), and (A.48), respectively.

References

Aoki, S. 1965, *Publ. Astron. Soc. Japan*, **17**, 273.

Aoki, S., and Iye, M. 1978, *Publ. Astron. Soc. Japan*, **30**, 519.

Bardeen, J. M. 1975, in *Dynamics of Stellar Systems, IAU Symp. No. 69*, ed. A. Hayli (Reidel Publ. Co., Dordrecht, Holland), p. 297.

Erdélyi, A., Magnus, W., Oberhettinger, F., and Tricomi, F. G. 1953, *Higher Transcendental Functions, Vol. 1* (McGraw-Hill, New York), chap. 3.

Erickson, S. A., Jr. 1974, unpublished Ph. D. thesis, M. I. T.

Francis, J. G. F. 1961a, *Comput. J.*, 4, 265.

Francis, J. G. F. 1961b, *Comput. J.*, 4, 332.

Fujimoto, M. 1968, in *Non Stable Phenomena in Galaxies, IAU Symp. No. 29*, ed. M. Arakelyan (Izdatel'stvo Akademii Nauk Armyanskoj SSR), p. 453.

Hohl, F. 1971, *Astrophys. J.*, **168**, 343.

Hunter, C. 1963, *Monthly Notices Roy. Astron. Soc.*, **126**, 299.

Hunter, C. 1965, *Monthly Notices Roy. Astron. Soc.*, **129**, 321.
Iye, M. 1978, *Publ. Astron. Soc. Japan*, **30**, 223.
Kalnajs, A. J. 1972, *Astrophys. J.*, **175**, 63.
Kalnajs, A. J. 1975, *La dynamique des galaxies spirales, Colloques Intern. CNRS. No. 241*, ed. L. Weliachew (Centre National de la Recherche Scientifique, Paris), p. 103.
Kuzmin, G. G. 1956, *Astron. Zh.*, **33**, 27.
Lau, Y. Y., Lin, C. C., and Mark, J. W.-K. 1976, *Proc. Natl. Acad. Sci. USA*, **73**, 1379.
Lin, C. C., and Shu, F. H. 1964, *Astrophys. J.*, **140**, 646.
Lin, C. C., Yuan, C., and Shu, F. H. 1969, *Astrophys. J.*, **155**, 721.
Lynden-Bell, D., and Kalnajs, A. J. 1972, *Monthly Notices Roy. Astron. Soc.*, **157**, 1.
Lynden-Bell, D., and Ostriker, J. P. 1967, *Monthly Notices Roy. Astron. Soc.*, **136**, 293.
Miller, R. H., Prendergast, K. H., and Quirk, W. J. 1970, *Astrophys. J.*, **161**, 903.
Miyamoto, M. 1969, *Publ. Astron. Soc. Japan*, **21**, 319.
Ostriker, J. P., and Peebles, P. J. E. 1973, *Astrophys. J.*, **186**, 467.
Takahara, F. 1978, *Publ. Astron. Soc. Japan*, **30**, 253.
Toomre, A. 1963, *Astrophys. J.*, **138**, 385.
Toomre, A. 1964, *Astrophys. J.*, **139**, 1217.
Toomre, A. 1969, *Astrophys. J.*, **158**, 899.